

This is an Open Access document downloaded from ORCA, Cardiff University's institutional repository: <https://orca.cardiff.ac.uk/id/eprint/152754/>

This is the author's version of a work that was submitted to / accepted for publication.

Citation for final published version:

Dulanya, Zuze, Gallen, Sean F., Kolawole, Folarin, Williams, Jack N., Wedmore, Luke N. J., Biggs, Juliet and Fagereng, Åke 2022. Knickpoint morphotectonics of the Middle Shire River basin: Implications for the evolution of rift interaction zones. *Basin Research* 34 (6) , pp. 1839-1858. 10.1111/bre.12687

Publishers page: <http://dx.doi.org/10.1111/bre.12687>

Please note:

Changes made as a result of publishing processes such as copy-editing, formatting and page numbers may not be reflected in this version. For the definitive version of this publication, please refer to the published source. You are advised to consult the publisher's version if you wish to cite this paper.

This version is being made available in accordance with publisher policies. See <http://orca.cf.ac.uk/policies.html> for usage policies. Copyright and moral rights for publications made available in ORCA are retained by the copyright holders.



# **Knickpoint Morphotectonics of the Middle Shire River Basin: Implications for the Evolution of Rift Interaction Zones**

Zuze Dulanya<sup>1</sup>, Sean F. Gallen<sup>2</sup>, Folarin Kolawole<sup>3</sup>, Jack N. Williams<sup>4,5,6</sup>, Luke N. J. Wedmore<sup>5</sup>,  
Juliet Biggs<sup>5</sup>, Åke Fagereng<sup>4</sup>

<sup>1</sup>*Geography and Earth Sciences Department, University of Malawi, Zomba, Malawi*

<sup>2</sup>*Department of Geosciences, Colorado State University, Fort Collins, CO, USA*

<sup>3</sup>*Lamont-Doherty Earth Observatory, Columbia University, Palisades, NY, USA*

<sup>4</sup>*School of Earth and Environmental Sciences, Cardiff University, Cardiff, UK*

<sup>5</sup>*School of Earth Sciences, University of Bristol, Bristol, UK*

<sup>6</sup>*Department of Geology, University of Otago, Dunedin, New Zealand*

## **Abstract**

Tectonic and paleo-environmental reconstructions of rift evolution typically rely on the interpretation of sedimentary sequences, but this is rarely possible in early-stage rifts where sediment volumes are low. To overcome this challenge, we use geomorphology to investigate landscape evolution and the role of different forcing mechanisms during basin development. Here, we focus on the humid Middle Shire River basin, located within the zone of progressive interaction and linkage between the southern Malawi Rift and Shire Rift Zone, East Africa. We used a digital elevation model to map knickpoints and knickpoint morphologies in the Middle Shire River basin and examined the relationships with pre-rift and syn-rift structures within the rift interaction zone. The main axial stream, Shire River, descends steeply, 372 m over a 50 km distance, across exposed metamorphic basement along the rift floor, exhibiting a strongly disequibrated

longitudinal elevation profile with both 'mobile' and 'fixed' knickpoints. In particular, we identify two clusters of mobile knickpoints, which we interpret as associated with baselevel fall events at the downstream end of the exposed basement that triggered knickpoint migration through the fluvial network since at least the Mid. Pleistocene. We infer that after the integration of the axial stream across the Middle Shire Basin, the knickpoints migrate upstream in response to fault-related subsidence in the Shire Rift Zone. Conversely, the fixed knickpoints are interpreted to reflect local differential bedrock erodibility at lithologic contacts or basement-hosted fault scarps along the basin floor. The results suggest that Middle Shire basin opening, associated with rift linkage, is likely a recent event (at least Mid. Pleistocene) relative to the Late Oligocene activation of Cenozoic rifting in the East African Rift's Western Branch. These findings support the hypothesis that the Western Branch developed from the gradual propagation, linkage, and coalescence of initially nucleated distinct rift basins.

**Keywords:** Knickpoints, Malawi Rift, Rift Interaction Zones; Tectonics

## Introduction

Landscape evolution is a complex process where quasi-equilibrium is maintained by a range of factors but particularly tectonism (Ebinger and Scholz, 2011; Burbank and Pinter, 1999) and climate (Tiercelin, 1990; Hartshorn et al., 2002; Bookhagen et al., 2005; Ferrier et al., 2013). In tectonically-active areas such as the East African Rift System (EARS), landscapes are highly dynamic, resulting in the interaction of various geomorphological processes (Bailey et al., 2000; Gawthorpe and Leeder, 2000; Flores-Prieto et al., 2015), including the progressive adjustment of the drainage networks to tectonic surface deformation. However, the interaction of climate and tectonics also complicates the process of environmental reconstruction, particularly in environments where suitable proxies are not available (Moore et al., 2009).

Early-stage rifts, where crustal thinning is minimal and magmatic systems are yet to develop (Ebinger et al., 2004; Chenin et al., 2018), are important for understanding the development of continental rifts as they set up the location of continental breakup margins. However, although seismic reflection datasets, commonly available in rifted margins, provide excellent images of the syn-rift stratigraphy, the typical low sediment volumes of early-stage rifting inhibit detailed investigation and paleoenvironmental reconstruction in these settings. Thus, active early-stage rift zones, such as the humid rift basins along the Western Branch of the East African Rift System, present an excellent opportunity to explore the salient geomorphic structure and landscape evolution peculiar to early-stage rifting. In such settings, geomorphic indicators such as drainage patterns, channel geometry, river behavior, knickpoints, and slope attitudes provide insights into the interactions between active crustal deformation and landscape

evolution (e.g., Vita-Finzi, 2012; Castillo et al., 2013; Kent et al., 2021; Gallen and Fernández-Blanco, 2021; Molin and Corti, 2015; Jiang et al., 2016).

Knickpoints are inflection points in longitudinal river profiles that demarcate a sudden change in river steepness steep sections along an otherwise smooth concave river profile, and are among some of the most widely used geomorphic features for the reconstruction of fluvial basin evolution and for the isolation of the roles of different forcing mechanisms (e.g. Phillips et al., 2010). Knickpoints can vary in form from short and discrete changes in river gradient (e.g. single waterfalls) to longer, higher-gradient segments extending for many kilometers also called knickzones (Whipple et al., 1999; Crosby and Whipple, 2006; Kirby and Whipple, 2012). Knickpoint formation is often triggered by a relatively sudden drop in river baselevel or change in baselevel fall rate that propagates throughout a fluvial network causing a transient response in the landscape (Castillo et al., 2013). However, the origins of knickpoints are not unique and can include tectonic movements, Quaternary glaciations, river captures, and local baselevel changes due to differential erosion between rocks of different competencies (Crosby and Whipple, 2006; Marrucci et al., 2018; Gallen et al., 2013; Gallen, 2018). Similar to other geomorphic proxies, the factors controlling knickpoint evolution may not always be independent or mutually exclusive (Boulton et al., 2014).

In this study, we investigated the mechanisms of landscape evolution in the humid Middle Shire River basin, hosted within a zone of tectonic interaction between the southern Malawi Rift and the Shire Rift Zone (Figures 1c-d). The study area is located along the Western Branch of the East African Rift system, where several studies hypothesize a model of rift growth by an initial nucleation of distinct rift basins that

gradually linked together (Ebinger et al., 1989; Nelson et al., 1992; Corti et al., 2007; Heilman et al., 2019; Kolawole et al., 2021; Jess et al., 2021). However, the details of landscape evolution within actively deforming rift interaction zones (RIZs) needed to test this hypothesis remain a longstanding knowledge gap. The Middle Shire's position between the southern Malawi Rift and Shire Rift Zone, and its youthful nature, as indicated by the sparseness of syn-rift deposits (Williams et al., 2022), indicates that it is an ideal natural laboratory for understanding how continental rifts progressively evolve in space and time.

We perform a geomorphic analysis by utilizing drainage pattern geometry and knickpoints to investigate the morphotectonics of the Middle Shire River basin. In doing so, we show how the axial stream morphology is guided by syn-rift faults, pre-existing basement lithological contacts, and changes in baselevel at the downstream end of the rift interaction zone. We then use features associated with the latter process to provide quantitative constraints on the possible timing of rift propagation and linkage across the rift interaction zone. The results of this study, therefore, advance the understanding of the spatio-temporal evolution of rift segment interaction and landscape evolution in continental rift zones.

## **2 The Middle Shire River Basin**

### **2.1 Location and Hydrology**

The study area is located in southern Malawi between latitudes 15° 30' S and 16° 00' S and bounded by the Malawi-Mozambique border to the west (approximately longitude 34°30' E) and longitude 35° 00' E to the east (Figures 1). The hydrology of southern Malawi is dominated by the Shire River, Malawi's largest river, and Lake Malawi's single outlet to the Zambezi River (Figure 1b, although it should be noted that ~90% of annual water loss from Lake Malawi is through evaporation (Drayton et al., 1984)). The river is critical to the country's socio-economic development as it supports irrigated agriculture and electricity generation. Electricity in Malawi is predominantly hydro-generated, with about 80% being produced from the Middle Shire section of the river (Taulo et al., 2015).

The Shire River is geographically divided into three main sections (Figure 1b), the Upper Shire (the northernmost segment), the Middle Shire, and the Lower Shire (the southernmost segment). The Upper Shire River runs from Lake Malawi at Mangochi (ca. 485 m above mean sea level (amsl)) to the Matope area (ca. 472 m amsl), following an arcuate bend in the Malawi Rift as it transitions from the NNW-trending Makanjira Graben to the NNE-SSW trending Zomba Graben (Figures 1b and c; Dulanya et al., 2017; Wedmore et al., 2020a; Williams et al., 2019, 2021). Along this section, the Shire River flows over unconsolidated alluvium and colluvium (Shela, 2000) and is characterized by meanders with a high sinuosity index (~1.17; Kolawole et al., 2021), reflecting the low topographic gradient (15 m) of the 130 km-distance between Mangochi and Matope. This lower gradient is also reflected by records of the Upper

129 Shire silting up in the early 20<sup>th</sup> century, and causing the upper 65 km section of the river  
130 to temporally flow back into Lake Malawi (Dixey 1924).

131 The boundary between the Upper and Middle Shire sections is where the river crosses  
132 the ENE-dipping Mlungusi Fault (Wedmore et al., 2020a) at Matope (ca. 472 m amsl,  
133 Figures 1b-d). At this point, the Shire River flows through a series of rapids and gorges  
134 that have recently been incised through basement rock to Chikwawa Town (at ca. 100  
135 m amsl), thus losing a height of nearly 380m over a distance of 50 km. This very steep  
136 gradient relative to the Upper Shire section results in a considerably lower sinuosity  
137 index (~1.04; Kolawole et al., 2021).

138 The Middle Shire River is characterized by erosion and narrow steep-sided river  
139 sections reflecting recent incision (Bloomfield and Garson, 1965a; Lister, 1967;  
140 Kolawole et al., 2021). A number of prominent rivers, some of which are tributaries of  
141 the Shire River, originate in the Middle Shire section, including the Lisungwe and  
142 Wamkurumadzi Rivers. These rivers have made deep incisions into the surrounding  
143 country rocks and reflect active denudational processes in the area. The course of the  
144 Lisungwe River in the area close to the Middle Shire section is deeply incised, occurring  
145 at a lower altitude than the Middle Shire River section. The differences in vertical  
146 heights between the two rivers in the Middle Shire section range from about 100 m near  
147 Matope to about 20 m near its confluence with the Shire River. Geological structure  
148 played a major role in the hydrology of this section in that the Shire and Lisungwe  
149 Rivers are fault-controlled for most of their parts (Bloomfield, 1965; Bloomfield and  
150 Garson, 1965a). Geomorphological evidence acquired from drainage morphology



seems to suggest that there has been drainage network reorganization that affected a number of rivers and streams whose watercourses have been redirected into or away from the Middle Shire since the Late Cretaceous/Early to Mid-Tertiary (Tweddle et al., 1979; Bloomfield and Young, 1961).

In the Lower Shire section, the Shire River meets the Mwanza River, which originates from the west near the border with Mozambique and flows along the Karoo-reactivated Mwanza Fault (e.g. Castaing 1991; Moore et al., 2007; Figure 1b). It may therefore reflect the original course of the Shire River prior to its linkage with the Upper Shire. The Lower Shire Section is characterized by a low gradient (~1 m elevation over 5 km distance), ox-bow lakes, meanders, and high sinuosity index (~1.28; Kolawole et al., 2021), similar to the Upper Shire section. Across this section, the Shire River flows southeast across the hanging-wall of the Thyolo Fault (Wedmore et al., 2020b) into a broad floodplain past Chikwawa Town and towards its confluence with the Zambezi River in Mozambique.

## **2.2 Climate**

Malawi has two main seasons; a cool dry season between May and October with a mean temperature of ~13 °C in June and July, and a hot wet season between November and April, where the mean temperature ranges between 30 and 35 °C (Nicholson et al., 2014). Rainfall is variable depending on altitude, ranging from 600 mm/yr on the rift valley floors to 1600 mm/yr in mountainous areas. The climate of the region is largely influenced by the seasonal migration and intensity of the intertropical convergence zone (ITCZ), a low-pressure belt within the Congo basin caused by tropical high-pressure belts over both the Indian and Atlantic Oceans (Nicholson, 2001;

Nicholson et al., 2014) and the Congo Air Boundary (CAB), controlled by sea-surface temperature (SST) anomalies such as the Indian Ocean Dipole (IOD) and El Niño/Southern Oscillation (ENSO) system (Abram et al., 2007; Saji et al., 1999).

General circulation models have shown that African climates are highly sensitive to high latitude glaciations (de Menocal, 1995; Gasse et al., 2008; Clark et al., 2009; Stone, 2014). For example, the Pleistocene-Holocene climate generally shows a succession of wet-dry cycles driven by global and regional circulation that affect the region with various patterns and intensities (e.g. Gasse, 2000; Filippi and Talbot, 2005; Thomas et al., 2009; Boxclaeer et al., 2012). Although the climate in the region is extremely variable, lake sediment cores from Lake Malawi, which forms the main catchment basin of the Shire River, have shown generally stable climate regimes for the last 75 ka (Scholz et al., 2007, 2011). This is unlike the 140–70 ka BP period which was characterized by megadroughts around 135–105 and 105–75 ka BP (Scholz et al., 2007, Konecky et al., 2011; Beuning et al., 2011).

### **2.3 Paleogeography**

Paleoclimate reconstructions show that the level of Lake Malawi has been highly variable since the Mid-Pleistocene (800–900 kyr) with lowstands of up to 600 m (Lyons et al., 2015, Ivory et al., 2016). However, over the last 75 ka of relative climate stability, the lake level has been relatively stable with consistent highstand conditions (levels 0–100 m below modern lake level; Scholz et al., 2007; Lyons et al., 2015).

The timing at which the Upper and Middle sections of the Shire River became an established connected river corridor and as Lake Malawi's main outlet are uncertain. The South Basin of Lake Malawi, which feeds the river, is thought to have evolved in the

Late Miocene – Mid. Pliocene (Scholz et al., 2020). Based on paleoenvironmental changes in Lake Malawi, Ivory et al. (2016) suggest that it was not until 800 Ka that the Shire River became Lake Malawi's main outlet. However, units of yellow to brown medium- to coarse-grained sands ranging in thickness from a few metres to hundreds of metres, known as the Chipalamawamba Beds, have been mapped in the vicinity of Lake Malombe (Figure 1a,b) and were dated to be Early – Mid. Holocene (van Boxclaer et al., 2012). The stratigraphic characteristics of these syn-rift deposits (van Boxclaer et al., 2012) suggest a lacustrine to riverine environment, interpreted to have been deposited during the development of the Shire River as Lake Malawi's outlet (van Boxclaer et al., 2012). Therefore, it is unclear if the Upper Shire began to drain Lake Malawi in the Mid-Pleistocene (~800 Ka) as suggested by Ivory et al. (2016) or the Early-Middle Holocene as suggested by van Boxclaer et al. (2012). The Lower Shire River is probably the oldest section of the Shire River which may have developed during the Permo-Triassic (Karoo) or Cretaceous phases of rifting in the Shire Rift Zone, associated with the Gondwana fragmentation (Castaing, 1991; Kolawole et al., 2022 preprint).

## **2.4 Geology and Tectonic Setting of Southern Malawi**

### **2.4.1 The Precambrian Basement**

The Middle Shire River Basin sits on a crystalline basement that is comprised of Proterozoic metamorphic rocks of both igneous and sedimentary parentage (Figure 2). These metamorphic rocks form part of the Southern Irumide orogenic belt (Mesoproterozoic age) that underwent amphibolite-granulite facies metamorphism

during the Pan-African Orogeny (~800-450 Ma.; Kröner et al., 2001; Fritz et al., 2013; Manda et al., 2019). Typical assemblages include various gneisses and charnockitic granulites of the Unango Terrane, part of the Mozambique Belt (Fullgraf et al., in press), with some intercalations of pelitic schists and paragneisses, calc-silicate rocks and marbles. Various orthogneissic rocks, including granitoid and basic orthogneisses, are associated with ring complexes found in the area (Bloomfield, 1958a; Bloomfield and Garson, 1965a, b; Walshaw, 1965; Evans, 1965; Habgood and Walshaw, 1965; Habgood, 1963; Morel, 1958). A prominent marble horizon is found along the amphibolite-granulite facies contact for nearly 40 km and forms a useful marker horizon of the boundary between these lithological units (Carter and Bennett, 1973).

#### **2.4.2 Phanerozoic Geology and structural History**

Structural studies in the south Malawi area indicate three main successive rift phases: the Karoo (NW-SE extension), the Cretaceous (NE-SW extension) and Cenozoic East African Rift System (ENE-WSW extension; Castaing, 1991; Wedmore et al. 2021). A sequence of Permian-Triassic sediments was deposited during Karoo rifting in the Lower Shire Graben (Habgood 1973, Castaing, 1991), but there is no evidence of Mesozoic sediments in the Upper and Middle Shire. In the Lower Jurassic, NE-SW striking Stormberg dolerite dykes were emplaced (Castaing, 1991) and then followed by a distinct period of upper Jurassic-Lower Cretaceous alkaline magmatism, which occurred throughout southern Malawi and is referred to as the Chilwa Alkaline Province (CAP; Bloomfield, 1965; Castaing, 1991; Dulanya, 2017; Eby et al., 1995; Woolley, 2001). Rocks of the CAP include syeno-granites, carbonatites, agglomerates, foidolites and associated alkaline dykes (Woolley, 2001) and are widespread within the study

area where they have a general ENE parallel strike to the Ntembwe Fault (Bloomfield and Garson, 1965a). Within the Lower Shire section, Cretaceous sandstones and marls belonging to the Lupata Group rest unconformably above the Karoo Group (Figure 2; Habgood and Walshaw, 1963; Habgood, 1965; Dixey, 1924).

## **2.5 Active Faulting and Quaternary Geology in the Middle Shire River Basin**

Geodetic models suggest that the southern Malawi Rift is currently accommodating 0.5-2 mm/yr ENE-WSW -oriented extension between the Rovuma and San Plates (Stamps et al., 2018; Wedmore et al., 2021). Rift-scale earthquake focal mechanism stress inversion also indicates a regional ENE-WSW-trending minimum compressive stress, although, at the scale of individual faults, local stress rotations are possible (Williams et al., 2019). The tectonic style of the Middle Shire is dominated by a set of curvilinear rift faults striking NW to N that extend northwards from the Lower Shire Graben Rift Zone to the Southern Malawi Rift's Zomba Graben (Figure 3; Kolawole et al., 2021). These are intersected by an orthogonal set of fractures with a NE-strike. The kinematics and geometry of these fractures are unclear, and the NE-striking fractures may be linked to the Karoo dolerite dyke emplacement, pre-existing metamorphic fabrics, poorly developed southwestward extension of the Zomba Graben faults, or extensional segments of a potential transverse NE-striking strike-slip fault in the Zomba Graben such as the Ntembwe Fault (Bloomfield and Garson, 1965a; Dulanya, 2017; Figure 3).

The Middle Shire River links the Zomba Graben and Lower Shire Graben (Ebinger et al., 1989; Lao-Davila et al., 2015; Dulanya et al., 2017; Williams et al., 2019; 2021; Wedmore et al., 2020a; Wedmore et al., 2020b; Kolawole et al., 2021). The two grabens

represent distinct rift sub-basins of which the former is in the Malawi Rift, oriented NNE, sits at a higher elevation, and hosts only Cenozoic syn-rift deposits; whereas the latter is in the Shire Rift Zone, oriented NW-SE, and hosts both Mesozoic and Cenozoic syn-rift deposits (Chisenga et al., 2019; Kolawole et al., 2022 preprint). The Lower Shire section of the rift is currently active with deformation hosted on reactivated Karoo faults (Castaing 1991; Chisenga et al., 2018; Wedmore et al., 2020b).

The Middle Shire section does not have well-developed basins for sediment deposition, which could be useful for disentangling its paleoenvironmental and tectonic history (Dulanya, 2017). Quaternary sediments are rare and thin (<100 m thick) in the Middle Shire area; however, assorted fluvio-lacustrine superficial deposits are present along major drainage features (Dulanya, 2017; Bloomfield and Garson, 1965a) and could provide evidence of the recent paleoenvironmental history of the area where they are present. Unconsolidated fluvial deposits previously described as black cotton clays (Morel, 1958) occur in an area about 5 km southwest of the Lisungwe-Shire River confluence covering an area of ca. 25 km<sup>2</sup> (Figure 2). The outcrop is elongated ~NNW-SSE, generally parallel to the strike direction of the prominent rift-related faults in the area. Despite the minimal late Cenozoic sedimentary record, the Middle Shire section possesses some remarkable geomorphotectonic features such as rapids, falls and gorges, which we investigate here for paleoenvironmental reconstructions.

### **3. Methodology**

In erosional landscapes, the shape of river profiles largely dictates topographic relief (e.g. Mackin, 1948; Morisawa, 1962; Gilbert, 1877). It has been shown that graded, equilibrated river profiles exhibit a power law scaling between local channel slope ( $S$ )

and upstream contributing drainage area ( $A$ ) (Morisawa, 1962; Flint, 1974; Kirby and Whipple, 2012), given by:

$$S = k_s A^{-\theta} \quad (\text{equation 1})$$

where  $\theta$  is the concavity index and  $k_s$  is the channel steepness index.

Because empirically calculated values of  $\theta$  and  $k_s$  covary, a reference concavity index ( $\theta_{ref}$ ) of  $\sim 0.45$ , typical of graded river profiles, allows for the calculation of the normalized steepness index ( $k_{sn}$ ) and the comparison of channel steepness across different drainage areas.

Simplified versions of the detachment-limited stream power model, which is appropriate for approximating long-term incision in bedrock channels, can be solved to arrive at a similar expression to equation 1. The detachment-limited stream power model simulates bedrock incision,  $E$ , as (Howard, 1994; Whipple and Tucker, 1999):

$$E = KA^m S^n \quad (\text{equation 2})$$

where  $K$  is an erodibility coefficient and  $m$  and  $n$  are positive constants that reflect aspects of basin hydrology, channel hydraulic geometry, and incision process, among other phenomena (Whipple, 2004). Equation 2 can be solved for local channel slope to show:

$$S = (E/K)^{1/n} A^{-m/n} \quad (\text{equation 3})$$

Comparison of equations 1 and 3 suggests that  $k_s$  or  $k_{sn} = (E/K)^{1/n}$  and  $\theta = -m/n$ . Noting that incision rates respond to rock uplift rates, at steady-state ( $E=U$ ), these relationships suggest that  $k_{sn}$  is a sensitive recorder of the spatial and temporal patterns of incision

rate and by association rock uplift rate (Snyder et al., 2000; Wobus et al., 2006; Anoop et al., 2012; Kirby and Whipple, 2012) but could also be affected by choice of the DEM (Boulton and Stokes, 2018) which could be a source of error in our work.

Typical values of  $m$  and  $n$  vary widely, but their ratio is typically between  $\sim 0.3$  and  $0.7$  (Snyder et al., 2000; Wobus et al., 2006; Kirby and Whipple, 2012), and some studies have shown that concavity index (e.g.,  $m/n$ ) increases with tectonic activity (Harel et al., 2016; Seybold et al., 2021) and decreases with increasing aridity (Harel et al., 2016; Chen et al., 2019). Regardless of these variations, the general consistency of the  $m$  to  $n$  ratio among numerous natural landscapes suggests that these parameters covary. The  $n$  parameter has been more widely studied than the  $m$  parameter, and in natural settings generally varies between  $0.5$  and  $4$  but might be as high as  $7$  (DiBiase and Whipple, 2011; Royden and Perron, 2013; Lague, 2014; Harel et al., 2016; Gallen and Wegmann, 2017; Gallen and Fernández-Blanco, 2021). Despite the wide range of reported values, most estimates of  $n$  are between  $1$  and  $2$ . For simplicity, later analyses conducted in this study assume that  $n = 1$ , but we recognize the limitations of this assumption.

The erodibility parameter,  $K$ , has been shown to vary over approximately 5 orders of magnitude (e.g., Stock and Montgomery, 1999; Harel et al., 2016). Variations in this parameter depend on a number of factors, including rock strength, climate, and sediment characteristics.

### **3.1 Stream profile extraction**



We used a Shuttle Radar Topography Mission (SRTM) digital elevation model (DEM) with a spatial resolution of 30 m to extract longitudinal stream profiles, performed using the MATLAB-based Topotoolbox (Schwangart and Scherler, 2014). The absolute vertical accuracy of the SRTM 30 m DEM is  $\leq 16$  m, and a relative accuracy is  $\leq 10$  m (Hensely et al., 2001). Apart from the stream profiles, this toolbox also generates flow directions, watershed boundaries and identifies knickpoints (Shahzad and Gloaguen, 2011a, b). The channel network was defined as portions of the landscape draining  $\geq 1$  km<sup>2</sup>. Elevation and drainage area extracted from the river network was then used to identify breaks in longitudinal channel slope as potential knickpoints (e.g. Zhang et al., 2017).

### 3.2 Knickpoint and knick zone mapping

Several computer-based algorithms have been developed based on the S-A power law relationships, useful for knickpoint mapping and analysis (e.g. Hayakawa and Oguchi, 2006; Wobus et al., 2006; Gonga-Saholiariliva et al., 2011; Queiroz et al., 2015; Zahra et al., 2017; Neely et al., 2017). In this work, we adopted the approach by Schwangart and Scherler (2014) because it closely mimics the early definitions of knickpoints (Gailleton et al., 2018). Knickpoints are identified along the longitudinal profiles of river tributaries using the *Knickpointfinder* function in TopoToolbox (Schwangart and Scherler, 2014). This is an iterative, automated procedure that identifies knickpoints as pronounced convex sections that separate concave equilibrium profiles in a DEM. The procedure achieves this by regressing linear segments of the streams in log S–log A space to provide a channel steepness index ( $k_s$ ) calculated from the upstream drainage area (1,000,000 km<sup>2</sup>) using the DEM and concavity ( $\theta = 0.45$ ) (Hack, 1957; Kirby and

Whipple, 2001; Snyder et al., 2000). Specifically, offsets between the actual river profile and a fitted concave-upward profile are identified as potential knickpoints (Stolle et al., 2019). Once these potential knickpoints are identified, we calculate normalized steepness index values, which are useful for the identification of true from false anomalies (knick zones), assuming the river profile was decreasing monotonously or not (Schwangart and Scherler, 2020).

### 3.3 Chi ( $\chi$ ) Analyses

Although the method described above is useful for extracting geomorphic parameters, the noise inherent in DEMs may mask some features of interest. For this reason, a statistical technique for quantifying the spatial variation called the chi ( $\chi$ ) analysis (Mudd et al., 2014) may be preferable. The  $\chi$ -parameter is calculated as the path integral along the channel of the inverse of drainage area ( $A(x)$ ) raised to the  $m$  to  $n$  ratio (i.e.,  $\theta_{ref}$ ) (Perron and Royden, 2013):

$$\chi = \int_{x_b}^x \left( \frac{A_o}{A(x)} \right)^{\frac{m}{n}} dx$$

(equation 4)

where  $A_o$  is an arbitrary reference drainage area used to give chi units of meters. This parameter can be used to examine the geometry of channels assuming that incision is equal to uplift where the slope of a  $\chi$ -elevation plot is proportional to  $k_{sn}$  (Perron and Royden, 2013; Mudd et al., 2014). The technique has the advantage of allowing for the comparison of the steepness of channels across basins of different sizes, and it is less

subject to topographic noise than slope-area analysis because the only inputs required are the drainage area and the elevation along the channel (Mudd et al., 2014).

These differences in  $\chi$ -values are used as an indication of which catchment basin is losing (lower  $\chi$ -values on one side of the divide) or gaining (higher  $\chi$ -values) catchment depending on either side of the divide (Willett et al., 2014). A disequilibrium state is found where  $\chi$ -values along rivers flowing in opposite sides of the drainage divide are not equal. A stable state is formed where the  $\chi$ -values are almost equal. Therefore  $\chi$ -maps have been used to show the growth and decay of drainage basins and have become a useful tool for understanding divide migration or equilibrium and disequilibrium conditions in catchment basins (Willett et al., 2014). Furthermore, we also used the  $\chi$ -values to determine the fluvial response time,  $\tau$ , by assuming  $n$  in the stream power model is 1:

$$\tau = \frac{\chi}{K^* A_0^{m/n}}$$

(equation 5)

The fluvial response time is then used to estimate knickpoint ages and migration rates from a common baselevel, which for our analyses is defined by the downstream ‘mouth’ of Middle Shire River near Chikwawa (Figure 6). Most of the published erodibility data present in the southern Africa region relates to loose soils and not derived for hard competent rocks like the ones for the study area (e.g. Vargas and Omuto, 2016; Gyamfi et al, 2016; Songu et al., 2021; Breetzke et al., 2013; Laker, 2004; Smith, 1999; Mughogho, unpublished). In this work, we used  $A_0 = 10^6 \text{ km}^2$  and a range of erodibility

( $K$ ) values of  $\sim 2 \times 10^{-6}$  to  $3 \times 10^{-6}$ , which were estimated by Jess et al. (2020) using thermochronology and river profile modelling for a roughly comparable rock type and climate from the Ruwenzori mountains farther north within the East African Rift system. In the absence of local constraints, we assume that these values are roughly representative of comparable rock units in the Middle Shire.

Using equation 4, the rate of knickpoint migration ( $r$ , in meters/year) can be estimated (equation 5) by the ratio of the knickpoint distance  $d$  from the point of propagation to its response time, given by:

$$r = \frac{d}{\tau}$$

*(Equation 6)*

The results obtained from these analyses have later been used for the interpretation of regional landscape evolution and correlations with the other spatial data, such as geological structures and precipitation that may be influencing knickpoint formation in the area (Fielding et al., 1994; Bookhagen and Burbank, 2006; Scotti et al., 2014; Azañón et al., 2015). In our study, we mark the base level location at the mouth of the Middle Shire River (at coordinate  $16.09^\circ$  S,  $34.86^\circ$  E which has an elevation of 70 m asl). Although the downstream mouth of the Middle Shire section receives inflow from both the Upper Shire and Middle Shire catchments (Figure 1c), we restricted the upstream drainage area ( $A_o$ ) used for our calculations to the Middle Shire river catchment. This approach was taken because taking the Upper Shire catchment into consideration would include the whole Lake Malawi catchment basin (Figure 1b). The

inclusion of the whole Lake Malawi catchment basin presents a problem as it creates an unreasonably large catchment area for the Middle Shire section. Thus, for our analysis, we treat the Middle Shire as an independent catchment, and we account for the uncertainties that this imposes on our estimates in the discussion part of this text (sections 5.4 and 5.5).

## **4 Results**

### **4.1 Knickpoint Analysis**

Results from the stream profile extraction (Figures 2, 3a-c) generally show a spatial correlation of knickpoints with fractures e.g. major faults, lithological units, metamorphic fabric and dykes (Figure 2, 3c).

We note here the following sequence in the spatial distribution of the knickpoints from the Upper to Lower Shire sections (Figures 3b, c):

- i.) From its contact with the Upper Shire segment at Matope, the first major knickpoint is at Murchison Falls (locality **i** on Figure 3b) with other knickpoints at Toni and Nachimbeya (locality **ii** on Figure 3b). The section between Matope and Mbinjewananda Rapids (located at **iii** on Figure 3b) roughly follows a NNE-SSW trend along the tectonic/lithologic boundary between the amphibolite and granulite facies suite characterized by a marble as a marker horizon between these two metamorphic suites (Figure 2). This boundary has also recently been described as the probable margin of the Southern Irumide and the Unango terranes (Fullgraf et al., in press). It appears that in this section, the course of the Shire River is largely controlled by geological features such as metamorphic fabrics e.g. foliation and some fractures

ii.) Between Mbinjewananda Rapids and the Shire River's confluence with the Lisungwe River, the former migrates away from the amphibolite-granulite contact and follows a SW-trend controlled by a mixture of fractures and various dykes. Along this section, the Shire River flows over two knickpoints (Nkula and Tedzani Falls, localities **iv** and **v** respectively in Figure 3b).

iii.) From its confluence with the Lisungwe, the Shire River switches to a largely SE trend, influenced by various fractures including the Lisungwe and Thyolo Faults and NE-SW to NW-SE striking geologic fabrics (Bloomfield and Garson 1965). Two knickpoints have formed either side of where the Shire River flows across an aplite dyke at Mpatamanga (localities **vi** and **vii** on Figure 3b).

iv.) A tectonic knickpoint has formed where the Shire River flows over the Thyolo fault near Chikwawa (locality **viii** at Kapichira on Figure 3b).

While we recognize that some of the knickpoints in the study area are likely static and associated with local features (i.e., faults or lithological contacts), we hypothesize that those that do not spatially correlate with these features might be mobile and related to periods of elevated base level drop at the base of the bedrock channels draining the Middle Shire. To test the hypothesis that pulses of incision are communicated throughout fluvial networks (Crosby and Whipple, 2006), we must first isolate static from presumably transient knickpoints. We test this using the chi analysis and the river response time analysis, which can determine if there are knickpoint sets that cluster in chi-elevation or  $\tau$ -elevation space. These clusters within this parameter space are significant because knickpoints migrate at the same rate vertically (so they will stay at

the same elevation if originating from the same base level fall event) and, assuming uniform erodibility, will also migrate at the same rate in  $\chi$ .

## 4.2 $\chi$ - analysis

From our analysis of the  $\chi$ -plot (Figure 4) it can be observed that  $\chi$ -values along specific stream channels emanating from the same drainage divide but constituting different catchment basins are different. From our analysis, the  $\chi$ -plot (Figure 4) shows different states of drainage divides, with most near the rift shoulders, and the Middle-to-Upper Shire boundary in a state of disequilibrium (unequal  $\chi$ -values on the opposite sides of a drainage divide) compared to the drainage divide between the Middle Shire and Lisungwe, which are in a steady-state (almost equal  $\chi$ -values on the opposite sides of a drainage divide). The histograms of knickpoint  $\chi$  and elevation (Figure 5) show a large spread (mean of ca. 110,000 and standard deviation of ca. 53,000  $\chi$ ) of the data ranging from ca. 17,000-265,000  $\chi$  occurring at altitudes of ca. 100 – 1400m asl (mean of about 700m asl with a standard deviation of 290m asl). However, we distinguish two main knickpoint clusters in the  $\chi$ -elevation distribution plots (Figure 5) whose main characteristics are summarized in Table 1. This result is important because mobile knickpoints migrate at the same rate vertically and in  $\chi$ -space provided spatially uniform rock uplift and erodibility (Niemann et al., 2001; Royden and Perron, 2013). The results for the modeled knickpoint migration rates in the Middle Shire River basin (Figures 6a and d), show values ranging between 0.06 to 2.0 m yr<sup>-1</sup> for different erodibility values (Figure 6a and d). Overall, the lower migration rates (<0.65 m yr<sup>-1</sup>) dominate the NW and SE margins of the basin, coinciding with the outer border fault zones, including the footwall areas of the Thyolo Fault. Whereas the highest migration rates (0.65–2.0 m yr<sup>-1</sup>)

<sup>1</sup>) occur mostly along and in the vicinity of the Middle Shire River channel along the basin axis.

The clustering indicates two broad time intervals i.e.ca. 51,000 – 124,000 years BP and ca. 99,000-210,000 years BP (Figures 6b and e) for the timing at which each set of knickpoint were formed.

***Table 1: Knickpoint response times and their K-values for the two clusters***

## **5 Discussions**

### **5.1 Local drainage dynamics**

The chi analysis map (Figure 4) shows that the drainage divides in the rift shoulder areas to the NW of Tedzani and near Blantyre together with the intrabasin area to the east of Matope are in a state of disequilibrium. These areas show that their drainage divides are migrating towards the axial stream of the Middle Shire River section. To the contrary, the axial stream of the Middle Shire section between Matope and Kapichira Falls covered by the Middle Shire and Lisungwe drainage divides are in a steady state. The clustering shown in the chi-elevation plots (Figure 5) also supports the idea that some tectonic activity is within the rift shoulder areas to the NW and SE. These observations suggest that most of the tectonic strain is accommodated in the axial region of the basin, which is consistent with previous fault mapping, rift morphology, and scarp offset distributions in this region (Wedmore et al., 2020a; Kolawole et al., 2021).

### **5.2 Knickpoints and formation mechanisms**



502 Consistencies in the location and form of knickpoints  
503 suggest a systematic response is responsible for their spatial distribution in the Middle  
504 Shire basin. The rapid incision in the Middle Shire area and localization of clusters in  
505 some sections of the border faults lead us to hypothesize that most of the strain in the  
506 region is localized within the axis of the Shire River where the river might be responding  
507 to baselevel fall associated with slip along the Thyolo Fault.

508 We identified both static and mobile knickpoints in the study area. The former are  
509 related to various faults, lithological contacts and metamorphic fabric, while the latter  
510 coincide with the outer border fault zones, including the footwall areas of the Thyolo  
511 Fault and the intrabasin faults near Matope (Figures 3 and 4). The locations of the static  
512 knickpoints suggest that these knickpoints are responding to variations in erodibility  
513 resulting in the formation of a step-like topography along the river pathways as is the  
514 present case in the course of the Middle Shire. The mobile knickpoints form two distinct  
515 clusters in chi-elevation space (Figure 5) and strongly support the notion that these  
516 knickpoints were triggered in response to baselevel fall events associated with tectonic  
517 perturbations along a fault downstream of the Middle Shire and cascade upstream  
518 through the fluvial network. The Thyolo Fault is the most prominent and fastest slipping  
519 fault downstream of the Middle Shire (Wedmore et al., 2020b; Williams et al., 2021),  
520 and so is most likely responsible for this baselevel fall. We do not rule out the possibility  
521 of contributions from tectonic subsidence in the active rift basins further downstream,  
522 such as the Nsanje graben (northern extension of the Urema Graben in central  
523 Mozambique; Dulanya, 2017). However, that the base level position near the Thyolo

fault does explain the mobile knickpoint pattern well (i.e. clustering in  $\chi$ -elevation space, Figures 5, 6a and c).

### **5.3 Migration Rates and Timing of formation of the Mobile Knickpoints**

Knickpoint modeling across the Middle Shire basin shows that the highest migration rates (Figures 6b and e) occur primarily along and in the vicinity of the Middle Shire axial stream channel and near the Thyolo Fault. This probably explains the proximity to the propagation centre (base level location) and that the basement rocks in the axial region of the Middle Shire river are being dismembered faster than in the other parts of the Middle Shire basin (i.e. rift shoulder).

The response times for the mobile knickpoints suggest they initiated between 51,000 to 210,000 years BP (Table 1) with two main clusters identified. We interpret that the older cluster (~99,000 and 210,000 years BP; Figures 6b-c, e-f) possibly corresponds to an earlier phase of increased slip rate along the Thyolo Fault during the Late to Middle Pleistocene, and that the second cluster corresponds to a another phase of increased slip rate along the fault (younger cluster timing of ~51,000 to 124,000 i.e. Late Pleistocene; Figures 6-c, e-f). Regardless of the interpretation of the older and younger clusters of mobile knickpoints, the fact that this record of slip rate perturbations along the Thyolo Fault exists in the Middle Shire basin implies an at least Mid. Pleistocene connection between the Middle Shire and Lower Shire basins. However, the exclusion of the Upper Shire catchment from the defined Middle Shire drainage area ( $A_o$ ) in our analysis implies a possible overestimation of the knickpoint response times and underestimation of the migration rates.

We acknowledge that this age estimate is sensitive to the erodibility constant  $K$  and this parameter, which is sensitive to the local climate and can only be inferred for southern Malawi. However, varying the full range of  $K$  values used in this calculation, as obtained from Jess et al., 2021 (i.e., between  $2 \times 10^{-6}$  and  $3 \times 10^{-6}$ ), does not substantially change the age estimates (Figure 6). Temporal variations in  $K$  may also exist in southern Malawi due to the occurrence of megadrought between 135 – 75 ka in the region (paleoclimate records in Lake Malawi sediment cores; Scholz et al., 2007). In these periods, lower incision rates of the bedrock rivers (due to reduced discharge and drainage area) would have decreased the rate of knickpoint retreat. Hence, our estimates of knickpoint migration rate represent an upper bound in the Middle Shire basin, and so basin linkage in southern Malawi could be slightly older than the Mid. Pleistocene (see equations 5 and 6). We infer that spatial variations in climate might explain some of the scatter in the knickpoint clusters.

We also acknowledge that there could have been some complexity in the spatiotemporal sequence of opening of the Middle Shire basin (i.e., north to south integration of the Shire River network), such as an initial opening of the Middle Shire to the Upper Shire prior to its linkage with the Lower Shire section, thus introducing some uncertainties into our age estimates. However, our interpretation of events is supported by syn-rift paleo-lake sediments at the southern end of the Zomba Graben including the Matope Beds and yet-to-be buried bedrock along the rift floor south of the Matope beds, suggesting a previously dammed southern-end of the Upper Shire segment (Bloomfield and Garson, 1965; Dulanya, 2017; Kolawole et al, 2021). Furthermore, an overall

southward propagation of long-term basin development at the scale of the Malawi Rift is consistent with previous studies (Scholz et al., 2020).

#### **5.4 Implications for Rift Interaction and Linkage in Southern Malawi**

We are thus able to propose a possible sequence of evolution of rift linkage and basin opening across the Middle Shire area (Figures 7a-b). Prior to the onset of East African Rifting in southern Malawi, the Upper and Middle Shire River sections were likely elevated basement regions relative to the Shire Rift Zone, which hosts the Lower Shire River, as only the latter experienced Karoo extension and subsidence (Bloomfield 1965; Habgood, 1973; Castaing, 1991). It has been suggested that prior to Cenozoic rifting in southern Malawi, the Upper Shire river might have flowed eastward into the Lake Chilwa basin, now located on the eastern rift flank (Figure 1c; Dixey, 1939). Considering the presence of more developed rift faulting and considerable syn-rift sediment deposits in the Upper Shire section (Malombe and Zomba grabens) relative to the Middle Shire area where both are lacking, rift basin development in the Upper Shire region likely preceded the propagation of rifting across the Middle Shire region. The Upper Shire rift faults may have developed relatively quickly (Plio-Pleistocene) to form a rift axis that channeled the axial Shire River southwards from Lake Malawi.

Thus, prior to the integration of the Upper and Lower Shire into a through-going trunk stream, the region of the Middle Shire River was an elevated unrifted basement that restricted flow in a closed-drainage system, and that at times may have resulted in paleo-lake formation in the Zomba Graben (Paleo-lake Matope; Figure 7a). This is represented by the presence of Cenozoic lacustrine clays and distinct large-scale beach

gravel deposits described as the Matope Beds which directly overlie the basement in the Zomba Graben (exposed on the footwall of the Mlungusi Fault; Bloomfield, 1965; Bloomfield and Garson 1965; Dulanya, 2017; Wedmore et al., 2020a). During this period, the predominant drainage along the Lower Shire section would have been the lower section of the Shire and Mwanza Rivers (Figure 7a; e.g. Moore et al., 2007), and the Lisungwe and Wamkurumadzi Rivers probably flowed eastwards (e.g. Bloomfield and Young, 1961; Bloomfield and Garson, 1965; Tweddle et al., 1979).

Subsequently, subsidence and tectonic movements along the Thyolo Fault in the Shire Rift Zone, and interactions with the southward propagating faults of the Southern Malawi Rift (e.g., Zomba, Lisungwe, and Chingale Step faults) led to surface deformation of the Middle Shire by the localization of rift interaction zone(RIZ)-breaching faults (Kolawole et al., 2021). Progressive faulting and erosion of the bedrock of the subsiding Middle Shire area resulted in the opening of the upper parts of the Middle Shire and re-routing of the course of the Shire River into a south-flowing axial stream leading to the linkage of the Zomba and Lower Shire basins (Figure 7b).

Within the bedrock stream network of the Middle Shire River, the southwest course of the northern part of the axial stream is parallel to the surrounding border and intrabasin faults of the Zomba Graben, whose geometry is strongly influenced by exploitation of basement metamorphic fabrics that are well oriented relative to regional EAR extension direction (Figure 7b; Mortimer et al., 2016; Williams et al., 2019; Kolawole et al., 2021). The southern half of the axial stream follows a southeast course, parallel to the trend of Thyolo Fault and a network of RIZ-breaching faults (Figure 7b) which also follow NW-trending basement fabrics (Wedmore et al., 2020b; Kolawole et al., 2021). Minor

deviations in the course of the Shire River downstream are influenced by other NE-trending fractures or lithological units, such as the aplite dyke at Mpatamanga gorge. Hence, the pre-existing basement fabrics have strongly influenced the brittle deformation and rift linkage between the Zomba and Lower Shire grabens.

Knickpoints are inherently transient features, particularly for rivers like the Shire with large drainage areas (Holland and Pickup, 1976; Crosby and Whipple, 2006; Hodge et al., 2020). In the bedrock drainage basin of the Middle Shire River, the preservation of multiple knickpoints across tectonic and lithologic discontinuities that we document here, and the Mid. to Late Pleistocene knickpoint response time suggest that the integration of the Middle and Lower Shire River sections is recent relative to the Oligocene-Miocene initiation of rifting in the region (Roberts et al., 2012; Ojo et al., 2022a). We note that the estimated ages of linkage is a lower bound considering that knickpoint formation must have occurred after basin linkage and that knickpoint migration rate may have been lower during well-documented Late Pleistocene (135-75 ka) megadrought period in the region (Scholz et al., 2007). Nevertheless, the results provide a minimum quantitative constraint on the timing of rift linkage between the southern Malawi Rift and Shire Rift Zone across the Middle Shire basin, which was only speculated on in previous studies of the Middle Shire RIZ (Dulanya et al., 2017; Kolawole et al., 2021).

More broadly, the results imply that the East African Rift western branch initiated and developed as distinct basins that have gradually linked together since the Late Oligocene rift activation in the region (Kolawole et al., 2021; Jess et al., 2021). We

suggest that the tectonic processes associated with the interaction and linkage of the Southern Malawi Rift and Shire Rift Zone facilitated the integration of the axial stream across the Middle Shire Basin. After rift linkage and starting in the Mid. Pleistocene, the knickpoints progressively began to migrate upstream in response to pulses of baselevel fall downstream of the Middle Shire River. This baselevel fall events are associated with active tectonic subsidence in the Lower Shire Graben, driven by slip along the Thyolo Fault.

## **6 Conclusions**

Landscape evolution responds to different forcing mechanisms at play in different parts of the Earth. In this study, we investigated the geomorphic evolution of the Middle Shire river basin in south Malawi, a bedrock river network which developed within a zone of rift interaction and linkage between the ~NNE-NNW-trending southern Malawi Rift and the NW-trending Shire Rift Zone. Despite its lack of well-developed basins with thick sediments, we utilize knickpoint mapping of bedrock rivers along the rift zone from a Digital Elevation Model (DEM) and analyze their associated geomorphic characteristics.

Our results show that the axial stream (Middle Shire River) exhibits a strong disequibrated longitudinal profile, and although inherited basement lithologic boundaries and faults modulate some of the knickpoint locations, there exist mobile knickpoints that are migrating upstream from through the river network due to base level fall events downstream in the Shire Rift Zone. We estimate a Mid. Pleistocene age for the oldest knickpoints in the network, representing a lower bound on the timing of integration of the Middle and Lower Shire River sections and rift linkage between the

southern Malawi Rift and Shire Rift Zone, relative to the Oligocene-Miocene initiation of rifting in the region.

More broadly, the results are consistent with the hypothesis that the East African Rift western branch has developed by the gradual propagation, linkage and coalescence of initially nucleated distinct rift basins. Further, the results show that the morphotectonic evolution of actively subsiding erosional rift floors in zones of recent rift segment linkage are influenced by inherited basement structures and syn-rift structures.

## **Acknowledgements**

We thank the editor Atle Rotevatn, and reviewers Sarah Boulton and Richard Ott for their constructive comments that helped to improve the quality of this paper. The field work component of the work was largely funded through the National Geographic Society (NGS) Grant Number CP-118R-17 to the first author. The corresponding knickpoint mapping desktop work was supported through a Benjamin Meaker fellowship grant to the first author by the University of Bristol. JW, LW, JB and AF are supported by EPSRC-Global Challenges Research Fund PREPARE (EP/P028233/1) and SAFER-PREPARED (part of the 'Innovative data services for aquaculture, seismic resilience and drought adaptation in East Africa' grant; EP/T015462/1) projects. Sincere thanks to both the NGS and University of Bristol for the generous support.



## References

- Abram, N., Gagan, M., Hantoro, W., McCulloch, M., Chappell, J., Suwargadi, B., 2007. Seasonal characteristics of the Indian Ocean Dipole during the Holocene epoch. *Nature*, 445: 299–302.
- Anoop, A., Prasad, S., Basavaiah, N., Brauer, A., Shahzad, F., Deenadayalan, K., 2012. Tectonic versus climate influence on landscape evolution: a case study from the upper Spiti valley, NW Himalaya. *Geomorphology* 145–146, 32–44.
- Azanon, J.M., Galve, J.P., Perez-Pena, J.V., Giaconia, F., Carvajal, R., Booth-Rea, G., Jabaloy, A., Vazquez, M., Azor, A., Roldan, F.J., 2015. Relief and drainage evolution during the exhumation of the Sierra Nevada (SE Spain): is denudation keeping pace with uplift? *Tectonophysics* 663, 19–32.
- Bailey, G., Manighetti, I., King, G., 2000. Tectonics, volcanism, landscape structure and human evolution in the African Rift. In: Bailey, G., Charles, R., Winder, N., Bailey, G., Charles, R., Winder, N. (Eds.), *Human Ecodynamics. Symposia of the Association for Environmental Archaeology*. Oxbow Books, pp. 31–46.
- Beuning, K.R.M., Zimmerman, K. A., Ivory, S. J., Cohen, A. S., 2011. Vegetation response to glacial–interglacial climate variability near Lake Malawi in the southern African tropics. *Palaeogeography, Palaeoclimatology, Palaeoecology* 303, 81–92.
- Bloomfield, K., Young, A., 1961. The geology and geomorphology of Zomba Mountain. *The Nyasaland Journal* 14, 54–80.

696 Bloomfield, K., 1958. The geology of the Port Herald area. *Bulletin of the Geological*  
697 *Survey of Malawi*, 9 (Government Printer, Zomba).

698 Bloomfield, K., 1965. The Geology of the Middle Shire Hydro-electric Power Sites in  
699 *Records of the Geological Survey of Malawi VII*, 29-44 (Government Printer, Zomba).

700 Bloomfield, K., Garson, M.S., 1965a. The geology of the Kirk Range-Lisungwe valley  
701 area. *Bulletin of the Geological Survey of Malawi*, 17 (Government Printer, Zomba).

702 Bloomfield, K., Garson, M.S., 1965b. The geology of the Zomba area. *Bulletin of the*  
703 *Geological Survey of Malawi*, 16 (Government Printer, Zomba).

704 van Bocxlaer, B., Salenbien, W., Praet, N., Verniers, J., 2012. Stratigraphy and  
705 paleoenvironments of the early to middle Holocene Chipalamawamba Beds (Malawi  
706 Basin, Africa). *Biogeosciences* 9, 4497-4512.

707 Bookhagen, B., Burbank, D.W., 2006. Topography, relief, and TRMM-derived rainfall  
708 variations along the Himalaya. *Geophysical Research Letters*, 33, 1–5.

709 Bookhagen, B., Thiede, R.C. and Strecker, M.R., 2005. Late Quaternary intensified  
710 monsoon phases control landscape evolution in the northwest Himalaya. *Geology*,  
711 33(2), 149-152.

712 Boulton, S.J., Stokes, M., 2018. Which DEM is best for analyzing fluvial landscape  
713 development in mountainous terrains? *Geomorphology* 310, 168-187.

714

715 Breetzke, G. D., Koomen, E., Critchley, W. R. S., 2013. GIS-assisted modelling in a  
716 South African catchment: Evaluating the USLE and SLEMSA Approach. In *Water*  
717 *Resources* by Ralph Wurbs (Ed.). Intertech Open.

718 Brune, S., Williams, S. E., Müller, R. D., 2018. Oblique rifting: the rule, not the  
719 exception. *Solid Earth* 9, 1187–1206.

720 Boulton, S. J., Stokes, M, Mather, A. E., 2014. Transient fluvial incision as an indicator  
721 of active faulting and Plio-Quaternary uplift of the Moroccan High Atlas. *Tectonophysics*,  
722 633, 16 – 33

723 Burbank, D.W. and Pinter, N., 1999. Landscape evolution: the interactions of tectonics  
724 and surface processes. *Basin Research*, 11(1), 1-6.

725 Carter, G.S., Bennet, J.D., 1973. The geology and mineral resources of Malawi. *Bulletin*  
726 *of the Geological Survey of Malawi*, 6 (Government Printer, Zomba).

727 Castaing, C., 1991. Post-Pan African tectonic evolution of South Malawi in relation to  
728 the Karoo and recent East African Rift Systems. *Tectonophysics*, 191(1–2), 55–73.

729 Castillo, M., Bishop, P., Jansen, J., 2013. Knickpoint retreat and transient bedrock  
730 channel morphology triggered by base-level fall in small bedrock river catchments: The  
731 case of the Isle of Jura, Scotland. *Geomorphology* 180–181:1–9

732 Chapola, L. S.; Kaphwiyo, C. E., 1992. The Malawi Rift: geology, tectonics and  
733 seismicity. *Tectonophysics* 209, 159-164

734 Chen, S.A., Michaelides, K., Grieve, S.W. and Singer, M.B., 2019. Aridity is expressed  
735 in river topography globally. *Nature*, 573(7775), pp.573-577

736 Chenin, P., Schmalholz, S.M., Manatschal, G. and Karner, G.D., 2018. Necking of the  
737 lithosphere: A reappraisal of basic concepts with thermo-mechanical numerical  
738 modeling. *Journal of Geophysical Research: Solid Earth*, 123(6), 5279-5299.

739 Chisenga, C., Dulanya, Z. and Jianguo, Y., 2019. The structural re-interpretation of the  
 740 Lower Shire Basin in the Southern Malawi rift using gravity data. *Journal of African*  
 741 *Earth Sciences*, 149, 280-290.

742 Chorowicz, J., 2005. The East African Rift System. *Journal of African Earth Sciences*,  
 743 43, 379-410. <https://doi.org/10.1016/j.jafrearsci.2005.07.019>

744 Clark, P. U., Dyke, A. S., Shakun, J. D., Carlson, A. E., Clark, J., Wohlfarth, B.,  
 745 Mitrovica, J. X., Hostetler, S. W. , McCabe, A. M., 2009. The Last Glacial Maximum.  
 746 *Science* 325: 710–714.

747 Cooper, W.G.G., Bloomfield, K., 1961. The geology of the Tambani-Salambidwe area.  
 748 *Bulletin of the Geological Survey of Malawi*, 13 (Government Printer, Zomba).

749 Corti, G., van Wijk, J., Cloetingh, S. and Morley, C.K., 2007. Tectonic inheritance and  
 750 continental rift architecture: Numerical and analogue models of the East African Rift  
 751 system. *Tectonics*, 26(6).

752 Crosby, B.T.; Whipple, K.X. 2006. Knickpoint initiation and distribution within fluvial  
 753 networks: 236 waterfalls in the Waipaoa River, North Island, New Zealand.  
 754 *Geomorphology* 82, 16–38.

755 Daly, M. C., Green, P., Watts, A. B., Davies, O., Chibesakunda, F., and Walker, R.,  
 756 2020. Tectonics and Landscape of the Central African Plateau and their Implications for  
 757 a Propagating Southwestern Rift in Africa. *Geochemistry, Geophysics,*  
 758 *Geosystems*, 21(6), e2019GC008746.

759 Daly, M.C., Chorowicz, J., Fairhead, J.D., 1989. Rift basin evolution in Africa: the  
760 influence of reactivated steep basement shear zones. In: Cooper, M.A., Williams, G.D.  
761 (Eds.), *Inversion Tectonics*, pp. 309-334. Geological Society Special Publications 44.

762 Dixey, F., 1924. Lake level in relation to rainfall and sunspots. *Nature* 2870(114), 659-  
763 661.

764 Dixey, F., 1939. The Early Cretaceous valley-floor peneplain of the Lake Nyasa region  
765 and its relation to tertiary rift structures. *Quart. J. geol. Soc., London*, 95, 75-108

766 Drayton, R. S. (1984). Variations in the level of Lake Malawi. *Hydrological Sciences*  
767 *Journal*, 29(1), 1-12.

768 Dulanya, Z., 2017. A review of the geomorphotectonic evolution of the south Malawi rift.  
769 *Journal of African Earth Sciences* 129, 728-738

770 Ebinger, C.J., 1989. Tectonic development of the western branch of the East African rift  
771 system. *Geological Society of America Bulletin*, 101(7), pp.885-903.

772 Ebinger, C., Scholz, C.A., 2011. Continental rift basins: the East African perspective,  
773 tectonics of sedimentary basins. John Wiley & Sons, Ltd, pp. 183–208.

774 Ebinger, C.J., Deino, A.L., Drake, R.E. and Tesha, A.L., 1989. Chronology of volcanism  
775 and rift basin propagation: Rungwe volcanic province, East Africa. *Journal of*  
776 *Geophysical Research: Solid Earth*, 94(B11), pp.15785-15803.

777 Eby G.N., Roden T. M., Krueger H.L., Ewing W., Faxon E.H., Woolley A.R., 1995.  
778 Geochronology and cooling history of the northern part of the Chilwa alkaline province,  
779 Malawi. *Journal of African Earth Sciences* 20: 275-288.

780 Evans, K., 1965. The geology of the Shire Highlands. *Bulletin of the Geological Survey*  
781 *of Malawi*, 18 (Government Printer, Zomba).

782 Ferrier, K.L., Huppert, K.L. and Perron, J.T., 2013. Climatic control of bedrock river  
783 incision. *Nature*, 496(7444), 206-209.

784 Filippi, M. L., Talbot, M. R., 2005. The palaeolimnology of northern Lake Malawi over  
785 the last 25ka based upon the elemental and stable isotopic composition of sedimentary  
786 organic matter. *Quaternary Science Reviews* 24, 1303–1328.

787 Flores-Prieto E, Quénéhervé, G., Bachofer, F., Shahzad, F., Maerker, M., 2015.  
788 Morphotectonic interpretation of the Makuyuni catchment in Northern Tanzania using  
789 DEM and SAR data. *Geomorphology* 248, 427–439

790 Fielding, E.J., Isacks, B.L., Barazangi, M., Duncan, C., 1994. How flat is Tibet? *Geology*  
791 22, 163-167.

792 Flint, J.J., 1974. Stream gradient as a function of order, magnitude, and discharge.  
793 *Water Resources Research* 10, 969-973.

794 Fullgraf, T., Dombola, K., Hyvonen, E., Thomas, B., and Zammit, C. (in press). The  
795 Provisional GEMMAP 1:1 Million Scale Structural and Geological Maps of Malawi:  
796 Geological Survey of Malawi.

797 Gailleton, B., Mudd, S. M., Clubb, F. J., Peifer, D., Hurst, M. D., 2019. A segmentation  
798 approach for the reproducible extraction and quantification of knickpoints from river long  
799 profiles. *Earth Surface Dynamics* 7, 211–230.

800 Gallen, S.F., Wegmann, K.W. and Bohnenstiehl, D.R., 2013. Miocene rejuvenation of  
801 topographic relief in the southern Appalachians. *GSA Today*, 23(2), 4-10.

802 Gallen, S.F., 2018. Lithologic controls on landscape dynamics and aquatic species  
803 evolution in post-orogenic mountains. *Earth and Planetary Science Letters* 493, 150-  
804 160.

805 Gallen, S.F. and Fernández-Blanco, D., 2021. A New Data-driven Bayesian Inversion of  
806 Fluvial Topography Clarifies the Tectonic History of the Corinth Rift and Reveals a  
807 Channel Steepness Threshold. *Journal of Geophysical Research: Earth Surface*,  
808 126(3), p.e2020JF005651

809 Gasse, F., 2000. Hydrological changes in the African tropics since the Last Glacial  
810 Maximum. *Quaternary Science Reviews*, 19, 189–211.

811 Gasse, F, Chalié, F, Vincens, A, Williams, M. A. J, Williamson, D., 2008. Climatic  
812 patterns in equatorial and southern Africa from 30,000 to 10,000 years ago  
813 reconstructed from terrestrial and near-shore proxy data. *Quaternary Science Reviews*  
814 27 (25–26): 2316–2340

815 Gawthorpe, R. L., and Leeder, M. R. (2000). Tectono-sedimentary evolution of active  
816 extensional basins. *Basin Research*, 12(3-4), 195-218.

817 Gilbert, G.: 1877. Geology of the Henry Mountains, USGS Unnumbered Series,  
818 Government Printing Office, Washington, D.C.

819 Goldrick, G., Bishop, P., 2007. Regional analysis of bedrock stream long profiles:  
820 evaluation of Hack's SL form, and formulation and assessment of an alternative (the DS  
821 form). *Earth Surface Processes and Landforms* 32, 649-671.

822 Gonga-Saholiariliva, N., Gunnell, Y., Harbor, D., and Mering, C., 2011. An automated  
823 method for producing synoptic regional maps of river gradient variation: Procedure,  
824 accuracy tests, and comparison with other knickpoint mapping methods,  
825 *Geomorphology* 134, 394–407.

826 Gyamfi, C, Ndambuki, J. M. and Salim, R.W., 2016. Spatial Variability Modeling of Soil  
827 Erodibility Index in Relation to  
828 Some Soil Properties at Field Scale. *Environment and Natural Resources Research*  
829 6(2), 16-27

830 Habgood, F., 1963. The geology of the country west of the Shire River between  
831 Chikwawa and Chiromo. *Bulletin of the Geological Survey of Malawi*, 14 (Government  
832 Printer, Zomba).

833 Habgood, F., Walshaw, R.D., 1965. The geology of the Cholo [Thyolo] area. *Bulletin of*  
834 *the Geological Survey of Malawi*, 22 (Government Printer, Zomba).

835 Hack, J. T., 1957. Studies of longitudinal stream profiles in Virginia and Maryland. In:  
836 US Geological Survey Professional Paper, 45-97.

837 Hartshorn, K., Hovius, N., Dade, W.B. and Slingerland, R.L., 2002. Climate-driven  
838 bedrock incision in an active mountain belt. *Science*, 297(5589), 2036-2038.

839 Hayakawa, Y. S. and Oguchi, T., 2006. DEM-based identification of fluvial knickzones  
840 and its application to Japanese mountain rivers, *Geomorphology* 78, 90–106.

841 Hecker, S., DeLong, S. B., and Schwartz, D. P., 2021. Rapid strain release on the Bear  
842 River fault zone, Utah–Wyoming—The impact of pre-existing structure on the rupture  
843 behavior of a new normal fault. *Tectonophysics*, 808, 228819.



844 Hensley, S., Munjy, R., Rosen, P., 2001. Interferometric synthetic aperture radar  
845 (IFSAR). *Digital elevation model technologies and applications: The DEM user's*  
846 *manual*, 143-206.

847 Hodge, M., Biggs, J., Fagereng, Å., Mdala, H., Wedmore, L. N. J., and Williams, J. N.,  
848 2020. Evidence from High-Resolution Topography for Multiple Earthquakes on High  
849 Slip-to-Length Fault Scarps: The Bilila-Mtakataka Fault, Malawi. *Tectonics*, 39(2),  
850 e2019TC005933.

851 Holland, W. N., and Pickup, G., 1976. Flume study of knickpoint development in  
852 stratified sediment. *Geological Society of America Bulletin* 87(1), 76-82.

853 Ivory, S. J., Blome, M. W., King, J. W., McGlue, M. M., Cole, J. E., and Cohen, A. S.,  
854 2016. Environmental change explains cichlid adaptive radiation at Lake Malawi over the  
855 past 1.2 million years. *Proceedings of the National Academy of Sciences*, 113 (42),  
856 11895-11900.

857 Jaiswara, N, J., Kotluri, S. K., Pandey, A.K., Pandey, P., 2019a. Transient basin as  
858 indicator of tectonic expressions in bedrock landscape: Approach based on MATLAB  
859 geomorphic tool (Transient-profiler). *Geomorphology* 346, 106853.

860 Jess, S., Koehn, D., Fox, M., Enkelmann, E., Sachau, T., and Aanyu, K. (2020).  
861 Paleogene initiation of the Western Branch of the East African Rift: The uplift history of  
862 the Rwenzori Mountains, Western Uganda. *Earth and Planetary Science Letters*, 552,  
863 116593.

864 Jiang, W., Han, Z., Zhang, J. and Jiao, Q., 2016. Stream profile analysis, tectonic  
865 geomorphology and neotectonic activity of the Damxung-Yangbajain rift in the south  
866 Tibetan Plateau. *Earth Surface Processes and Landforms*, 41(10), 1312-1326.

867 Joyce, A. A., Mueller, R. G., 1992. The social impact of anthropogenic landscape  
868 modification in the Río Verde drainage basin, Oaxaca, Mexico. *Geoarchaeology*, 7(6),  
869 503-526.

870 Katumwehe, A. B., Abdelsalam, M. G., Atekwana, E. A., 2015. The role of pre-existing  
871 Precambrian structures in rift evolution: The Albertine and Rhino grabens,  
872 Uganda. *Tectonophysics*, 646, 117-129.

873 Keller, G. R., Morgan, P., Seager, W. R., 1990. Crustal structure, gravity anomalies and  
874 heat flow in the southern Rio Grande rift and their relationship to extensional  
875 tectonics. *Tectonophysics*, 174(1-2), 21-37.

876 Kent, E., Boulton, S.J., Whittaker, A.C., Stewart, I.S. and CihatAlçiçek, M., 2017.  
877 Normal fault growth and linkage in the Gediz (Alaşehir) Graben, Western Turkey,  
878 revealed by transient river long-profiles and slope-break knickpoints. *Earth Surface*  
879 *Processes and Landforms*, 42(5), 836-852.

880 Kirby, E., Whipple, K. X., 2001. Quantifying differential rock-uplift rates via stream profile  
881 analysis. *Geology* 29, 415-418.

882 Kirby, E., Whipple, K. X., 2012. Expression of active tectonics in erosional landscapes.  
883 *Journal of Structural Geology* 44, 54-75

884 Knight, J., Stratford, D., Grab, S. W. 2016. Landscape–climate–human interactions in  
885 southern Africa. In: Knight, J. and Grab, S.W. (eds) Quaternary environmental change

886 in southern Africa: physical and human dimensions. Cambridge University Press, 412-  
887 431.

888 Kolawole, F., Vick, T., Atekwana, E.A., Laó-Dávila, D.A., Costa, A.G., and Carpenter,  
889 B.M. (2022 preprint). Strain Localization and Migration During the Pulsed Lateral  
890 Propagation of the Shire Rift Zone, East Africa. Doi: 10.1002/essoar.10510192.1.  
891 ESSOAr preprint: <https://www.essoar.org/doi/abs/10.1002/essoar.10510192.1>

892 Kolawole, F., Firkins, M. C.; Al Wahaibi, T. S., Atekwana, E. A., Soreghan, M. J., 2021.  
893 Rift Transfer Zones and the Stages of Rift Linkage in Active Segmented Continental Rift  
894 Systems, *Basin Research*, 33(6), 2984-3020.

895 Korup, O., 2006. Rock-slope failure and the river long profile. *Geology* 34, 45-48.

896 Kroner, A., 1993. The Pan-African Belt of Northeastern and Eastern Africa,  
897 Madagascar, Southern India, Sri Lanka and East Antarctica: Terrane Amalgamation  
898 during the Formation of the Gondwana Supercontinent. In: Thornweihe, U.,  
899 Schandelmeier, H. (Eds.), *Geoscientific Research in Northeast Africa*. Balkema,  
900 Rotterdam, pp. 3-9.

901 Kroner, A., Willner, A.P., Hegner, E., Jaeckel, P., Nemchin, A., 2001. Single zircon  
902 ages, PT evolution and Nd isotopic systematics of high-grade gneisses in southern  
903 Malawi and their bearing on the evolution of the Mozambique belt in southeastern  
904 Africa. *Precambrian Research* 109, 257-291.

905 Laker, M. C., 2004. Advances in soil erosion, soil conservation, land suitability  
906 evaluation and land use planning research in South Africa, 1978-2003. *S. Afr. 1. Plant*  
907 *Soil* 21 (5), 345-368.

908 Laó-Dávila, D. A., Al-Salmi, H. S., Abdelsalam, M. G., and Atekwana, E. A., 2015.  
 909 Hierarchical segmentation of the Malawi Rift: The influence of inherited lithospheric  
 910 heterogeneity and kinematics in the evolution of continental rifts. *Tectonics*, 34, 2399-  
 911 2417.

912 Lister, L. A., 1967. Erosion surfaces in Malawi. Records VII, *Geological Survey of*  
 913 *Malawi*.

914 Macgregor, D., 2015. History of the development of the East African Rift System: A  
 915 series of interpreted maps through time. *Journal of African Earth Sciences* 101, 232–  
 916 252

917 Mackin, J. H., 1948. Concept of the graded river. *GSA Bulletin* 59, 463–512.

918 Manda, B. W., Cawood, P. A., Spencer, C. J., Prave, T., Robinson, R., & Roberts, N. M.  
 919 (2019). Evolution of the Mozambique Belt in Malawi constrained by granitoid U-Pb, Sm-  
 920 Nd and Lu-Hf isotopic data. *Gondwana Research*, 68, 93-107.

921 Marrucci, M., Zeilinger, G., Ribolini, A., Schwanghart, W., 2018. Origin of Knickpoints in  
 922 an Alpine Context Subject to Different Perturbing Factors, Stura Valley, Maritime Alps  
 923 (North-Western Italy). *Geosciences* 8(12), 443-

924 de Menocal, P. B., 1995. Plio-Pleistocene African climate. *Science*, 270, 53–59

925 Molin, P. and Corti, G., 2015. Topography, river network and recent fault activity at the  
 926 margins of the Central Main Ethiopian Rift (East Africa). *Tectonophysics*, 664, 67-82.

927 Morley, C. K., Cunningham, S. M., Harper, R. M., and Wescott, W. A., 1992. Geology  
 928 and geophysics of the Rukwa rift, East Africa. *Tectonics* 11(1), 69–81.

929  
 930 Moore, A.E., Coterrill, F.P.D., Mian, M.P.L., Williams, H.B., 2007. The Zambezi River.  
 931 In: Gupta, A. (Ed.), *Large Rivers: Geomorphology and Management*. John Wiley and  
 932 Sons Ltd, London, pp. 311-332.

933 Moore, A., Blenkinsop, T., Cotterill, F., 2009. Southern African topography and erosional  
 934 history: Plumes or plate tectonics? *Terra Nova* 21, 310-315.

935 Morel, S.W., 1958. The geology of the Middle Shire Area. *Bulletin of the Geological*  
 936 *Survey of Nyasaland [Malawi]* 10.

937 Mortimer, E. J., Paton, D. A., Scholz, C. A., Strecker, M. R., 2016. Implications of  
 938 structural inheritance in oblique rift zones for basin compartmentalization: Nkhata Basin,  
 939 Malawi Rift (EARS). *Marine and Petroleum Geology* 72, 110-121

940 Mudd, S. M., Attal, M., Milodowski, D. T., Grieve, S. W. D., Valters, D. A., 2014. A  
 941 statistical framework to quantify spatial variation in channel gradients using the integral  
 942 method of channel profile analysis. *Journal of Geophysical Research: Earth Surface*,  
 943 119, 138–152.

944 Mughogho, M. T. (1998). Evaluation of the Revised Universal Soil Loss Equation  
 945 (RUSLE) and the Soil Loss Estimation Model for Southern Africa (SLEMSA) Under  
 946 Malawi Conditions: A Case Study of Kamundi Catchment Near Mangochi. Unpublished  
 947 BSc Dissertation, University of Malawi.  
 948 <https://cals.arizona.edu/oals/malawi/Papers/Mughogho98.html>

949 Neely, A. B., Bookhagen, B., Burbank, D. W., 2017. An automated knickzone selection  
 950 algorithm (KZ-Picker) to analyze transient landscapes: Calibration and validation,  
 951 <https://doi.org/10.1002/2017JF004250>, 2017

952 Nichols, G., 2013. Sedimentology and stratigraphy. Wiley (423 pp.).

953 Nicholson, S. E., Klotter, D., Chavula, G., 2014. A detailed rainfall climatology for  
 954 Malawi, Southern Africa. *International Journal of Climatology*, 34: 315–325.

955 Nicholson, S. E., 2001. Climatic and environmental change in Africa during the last two  
 956 centuries. *Climate Research* 17, 123 –144

957 Niemann, J.D., Gasparini, N.M., Tucker, G.E. and Bras, R.L., 2001. A quantitative  
 958 evaluation of Playfair's law and its use in testing long-term stream erosion models. *Earth*  
 959 *Surface Processes and Landforms: The Journal of the British Geomorphological*  
 960 *Research Group*, 26(12), 1317-1332.

961 Ojo, O. O., Thomson, S., Laó-Dávila, D. A.(2022a preprint). Neogene-Quaternary  
 962 Initiation of the Southern Malawi Rift linked to Reactivation of the Carboniferous-  
 963 Jurassic Shire Rift.  
 964 ESOARpreprint:<https://www.essoar.org/doi/abs/10.1002/essoar.10511357.1>

965 Ojo, O.O., Ohenhen, L.O., Kolawole, F., Johnson, S.G., Chindandali, P.R., Atekwana,  
 966 E.A. and Laó-Dávila, D.A. (2022b). Under-displaced normal faults: Strain  
 967 accommodation along an early-stage rift-bounding fault in the Southern Malawi Rift.  
 968 *Frontiers in Earth Science*, 10.

969 Olive, J. A., Behn, M. D., Malatesta, L. C. (2014). Modes of extensional faulting  
 970 controlled by surface processes. *Geophysical Research Letters*, 41(19), 6725-6733.

971 Perron, J. T. and Royden, L., 2013. An integral approach to bedrock river profile  
 972 analysis. *Earth Surface Processes and Landforms*, 38, 570–576,  
 973 <https://doi.org/10.1002/esp.3302>.

974 Phillips, J.D.; McCormack, S.; Duan, J.; Russo, J.P.; Schumacher, A.M.; Tripathi, G.N.;  
 975 Brockman, R.B.; Mays, A.B.; Pulugurtha, S., 2010. Origin and interpretation of  
 976 knickpoints in the Big South Fork River basin, Kentucky–Tennessee. *Geomorphology*  
 977 114, 188–198.

978 Queiroz, G. L., Salamuni, E., and Nascimento, E. R, 2015. Knickpoint finder: A software  
 979 tool that improves neotectonic analysis. *Computers and Geosciences* 76, 80–87.

980 Rickets, R. D., Johnson, T. C., 1996. Early Holocene changes in lake level and  
 981 productivity in Lake Malawi as interpreted from Oxygen and carbon isotopic  
 982 measurements of authigenic carbonates. In: The limnology, climatology and  
 983 paleoclimatology of the East African Lakes. Edited by Johnson, T. C. and Odada E. O.,  
 984 Gordon and Breach, Amsterdam, 475-493

985 Roberts, E. M., Stevens, N. J., O'Connor, P. M., Dirks, P. H. G. M., Gottfried, M.D.,  
 986 Clyde, W.C., Armstrong, R.A., Kemp, A.I.S., and Hemming, S., 2012. Initiation of the  
 987 western branch of the East African Rift coeval with the eastern branch. *Nature*  
 988 *Geoscience* 5(4), 289-294.

989 Rosendahl, B.R., Kilembe, E., Kaczmarick, K., 1992. Comparison of the Tanganyika,  
 990 Malawi, Rukwa and Turkana Rift zones from analyses of seismic reflection data.  
 991 *Tectonophysics* 213, 235-256.

992 Royden, L. and Taylor Perron, J., 2013. Solutions of the stream power equation and  
 993 application to the evolution of river longitudinal profiles. *Journal of Geophysical*  
 994 *Research: Earth Surface*, 118(2), 497-518.

995 Saji, N.H., Goswami, B.N., Vinayachandran, P.N., and Yamagata, T., 1999. A dipole  
 996 mode in the tropical Indian Ocean. *Nature* 401, 360–363.

997 Schwanghart, W., Scherler, D., 2014. TopoToolbox 2—MATLAB-based software for  
 998 topographic analysis and modelling in Earth surface sciences. *Earth Surface Dynamics*  
 999 2, 1-7.

1000 Scherler, D., Schwanghart, W., 2020a. Drainage divide networks – Part 1: Identification  
 1001 and ordering in digital elevation models. *Earth Surface Dynamics* 8, 245–259.

1002 Schwanghart, W., and Scherler, D., 2020b, Drainage divide networks – Part 2:  
 1003 Response to perturbations. *Earth Surface Dynamics* 8, 261–274.

1004 Schwanghart, W., and Scherler, D., 2020, Divide mobility controls knickpoint migration  
 1005 on the Roan Plateau (Colorado, USA): *Geology*, 48.

1006 Schoenbohm, L.M., Whipple, K.X., Burchfiel, B.C., Chen, L., 2004. Geomorphic  
 1007 constraints on surface uplift, exhumation, and plateau growth in the Red River region,  
 1008 Yunnan Province, China. *Geological Society of America Bulletin* 116 (7), 895.



1009 Scholz, C. A., Johnson, T. C., Cohen, A. S., King, J. W., Peck, J. A., Overpeck, J. T.,  
 1010 Talbot, M. R., Brown, E. T., Kalindekaffe, L., Amoako, P. Y. O., Lyons, R. P., Shanahan,  
 1011 T. M., Castaneda, I. S., Heil, C. W., Forman, S. L., Mchargue, L. R., Beuning, K. R.,  
 1012 Gomez, J., Pierson, J., 2007. East African Mega-droughts between 135 and 75  
 1013 Thousand Years Ago and Bearing on Early-modern Human Origins. *PNAS* 104/42,  
 1014 16416-16421.

1015 Scholz, C. A., Cohen, A. S., Johnson, T. C., King, J., Talbot, M. R., & Brown, E. T.  
 1016 (2011). Scientific drilling in the Great Rift Valley: the 2005 Lake Malawi Scientific Drilling  
 1017 Project—an overview of the past 145,000 years of climate variability in Southern  
 1018 Hemisphere East Africa. *Palaeogeography, Palaeoclimatology, Palaeoecology*, 303(1-  
 1019 4), 3-19.

1020 Scotti, V.N., Molin, P., Faccenna, C., Soligo, M., Casas-Sainz, A., 2014. The influence  
 1021 of surface and tectonic processes on landscape evolution of the Iberian Chain (Spain):  
 1022 quantitative geomorphological analysis and geochronology. *Geomorphology* 206, 37–  
 1023 57.

1024 Seybold, H., Berghuijs, W.R., Prancevic, J.P. and Kirchner, J.W., 2021. Global  
 1025 dominance of tectonics over climate in shaping river longitudinal profiles. *Nature*  
 1026 *Geoscience*, 14(7), pp.503-507.

1027 Shahzad, F., Gloaguen, R., 2011a. TecDEM: a MATLAB based toolbox for tectonic  
 1028 geomorphology, Part 1: drainage network preprocessing and stream profile analysis.  
 1029 *Computers in Geosciences* 37 (2), 250–260.

1030 Shahzad, F., Gloaguen, R., 2011b. TecDEM: a MATLAB based toolbox for tectonic  
 1031 geomorphology, part 2: surface dynamics and basin analysis. *Computers in*  
 1032 *Geosciences*. 37(2), 261–271.

1033 Shela, O., 2000. In: Naturalisation of Lake Malawi Levels and Shire River Flows:  
 1034 Challenges of Water Resources Research and Sustainable Utilisation of the Lake  
 1035 Malawi - Shire River System. 1<sup>st</sup> WARFSA/ WaterNet Symposium: Sustainable Use of  
 1036 Water Resources, Maputo, 1-2 November 2000. <http://www.bscw.ihe.nl/pub/bscw.cgi>.

1037 Sherman, S. I., 1992. Faults and tectonic stresses of the Baikal rift  
 1038 zone. *Tectonophysics*, 208(19921), 297-307.

1039 Smets, B., Delvaux, D., Ross, K. A., Poppe, S., Kervyn, M., d'Oreye, N., Kervyn, F.,  
 1040 2016. The role of inherited crustal structures and magmatism in the development of rift  
 1041 segments: Insights from the Kivu basin, western branch of the East African  
 1042 Rift. *Tectonophysics* 683, 62-76.

1043 Smith, H. J., 1999. Application of empirical soil loss models in Southern Africa: a review.  
 1044 *S. Afr. Tydskr. Plant Grond* 16(3), 158-163.

1045 Snyder, N.P., Whipple, K.X., Tucker, G.E., Merritts, D.J., 2000. Landscape response to  
 1046 tectonic forcing: digital elevation model analysis of stream profiles in the Mendocino  
 1047 triple junction region, northern California. *Geological Society of America Bulletin* 112 (8),  
 1048 1250–1263.

1049 Songu, G.A., Abu, R.D., Temwa, N.M., Yiye, S.T., Wahab, S., Mohammed, B. G., 2021.  
 1050 Analysis of soil erodibility factor for hydrologic processes in Kereke watershed, North

1051 Central Nigeria. *Journal of Applied Sciences and Environmental Management* 25(3),  
 1052 425-432.

1053 Stolle A., Schwanghart, W., Andermann, C., Bernhardt, A., Fort, M., Jansen, J. D.,  
 1054 Wittmann, H., Merchel, S., Rugel, G., Adhikari, B. R., Korup, O., 2019. Protracted river  
 1055 response to medieval earthquakes. *Earth Surface Processes and Landforms* 44: 331–  
 1056 341.

1057 Stone, A. E. C., 2014. Last Glacial Maximum conditions in southern Africa: Are we any  
 1058 closer to understanding the climate of this time period? *Progress in Physical*  
 1059 *Geography: Earth and Environment* 38(5), 519-542.

1060 Taulo, J. L., Gondwe, K. J., Sebitosi, A. B., 2015. Energy supply in Malawi: Options and  
 1061 issues. *Journal of Energy in Southern Africa* 26(2), 19–32).

1062 Telbisz, T., Kovács, G., Székely, B., Szabó, J., 2013. Topographic swath profile  
 1063 analysis: a generalization and sensitivity evaluation of a digital terrain analysis tool.  
 1064 *Zeitschrift für Geomorphologie* 57(4), 485–513

1065 Tiercelin, J.J., 1990. Rift-basin sedimentation: responses to climate, tectonism and  
 1066 volcanism. Examples of the East African Rift. *Journal of African Earth Sciences* 10 (1–  
 1067 2), 283–305.

1068 Vargas, R. and Omuto, C., 2016. Soil loss  
 1069 assessment in Malawi. Food and Agriculture Organization of the United Nations, 1-60.  
 1070 [https://info.undp.org/docs/pdc/Documents/H21/Soil%20Loss%20ReportFinal%20copy%](https://info.undp.org/docs/pdc/Documents/H21/Soil%20Loss%20ReportFinal%20copy%20November%202018,%202016.pdf)  
 1071 [20November%2018,%202016.pdf](https://info.undp.org/docs/pdc/Documents/H21/Soil%20Loss%20ReportFinal%20copy%20November%202018,%202016.pdf)

1072 Vita-Finzi, C., 1966. River history and tectonics. *Philosophical Transactions of The*  
1073 *Royal Society A Mathematical Physical and Engineering Sciences* 370: 2173-92

1074 Walshaw, R.D., 1965. The geology of the Ntcheu-Balaka area. *Bulletin of the Geological*  
1075 *Survey of Malawi*, 19 (Government Printer, Zomba).

1076 Wedmore, L. N. J., Biggs, J., M. Floyd, Fagereng, Å, Mdala, H., Chindandali, P.,  
1077 Williams, J. N., Mphepo, F., 2021. Geodetic Constraints on Cratonic Microplates and  
1078 Broad Strain during Rifting of Thick Southern African Lithosphere. *Geophysical*  
1079 *Research Letters* 48 (17), <https://doi.org/10.1029/2021GL093785>

1080 Wedmore, L. N. J., Biggs, J., Williams, J. N., Fagereng, Å., Dulanya, Z., Mphepo, F.,  
1081 and Mdala, H., 2020a. Active fault scarps in southern Malawi and their implications for  
1082 the distribution of strain in incipient continental rifts. *Tectonics*, 39, e2019TC005834.  
1083 <https://doi.org/10.1029/2019TC005834>

1084 Wedmore, L. N. J., Williams, J. N., Biggs, J., Fagereng, Å., Mphepo, F., Dulanya, Z.,  
1085 Willoughby, J., Mdala, H., Adams, B., 2020b. Depth-dependent controls on structure,  
1086 reactivation and geomorphology of the active Thyolo border fault, Malawi rift. *Journal of*  
1087 *Structural geology*. <https://doi.org/10.31223/osf.io/4bs9x>

1088 Whipple, K. X., Kirby, E., and Brocklehurst, S. H., 1999. Geomorphic limits to climate-  
1089 induced increases in topographic relief. *Nature*, 401, 39–43.

1090 Whipple, K. X., DiBiase, R. A., and Crosby, B. T., 2013. Bedrock Rivers, in: Treatise on  
1091 Geomorphology, edited by: Shroder, J. F., Academic Press, San Diego, 550–573.

1092 van Wijk, W., Blackman, D.K., 2005. Dynamics of continental rift propagation: the end-  
1093 member modes. *Earth and Planetary Science Letters* 229, 247–258.

1094 Willett, S. D., McCoy, S. W., Taylor Perron, J., Goren, L., and Chen, C. Y., 2014.  
 1095 Dynamic reorganization of River Basins, *Science* 343, 1248765,  
 1096 <https://doi.org/10.1126/science.1248765>.

1097 Williams, J. N., Fagereng, A., Wedmore, L., Biggs, J., Mphepo, F., Dulanya, Z., Mdala,  
 1098 H., Blenkinsop, T., 2019. How do variably striking faults re-activate during rifting?  
 1099 Insights from southern Malawi? *G-Cubed* <https://doi.org/10.1029/2019GC008219>.

1100 Williams, J. N., Mdala, H., Fagereng, Å., Wedmore, L. N., Biggs, J., Dulanya, Z.,  
 1101 Chindandali, P., Mphepo, F., 2021. A systems-based approach to parameterize seismic  
 1102 hazard in regions with little historical or instrumental seismicity: active fault and  
 1103 seismogenic source databases for southern Malawi. *Solid Earth*, 12(1), 187-217.

1104 Williams, J.N.; Wedmore, L.N.J.; Scholz, C.A.; Kolawole, F.; Wright, L.J.M.; Shillington,  
 1105 D. J.; Fagereng, Å., Biggs, J., Mdala, H., Dulanya, Z., Mphepo, F., Chindandali, P.,  
 1106 Werner, M.J., 2022. The Malawi Active Fault Database: an onshore-offshore database  
 1107 for regional assessment of seismic hazard and tectonic evolution. *G-Cubed*. 23 (5), 1-  
 1108 25. <https://doi.org/10.1029/2022GC010425>

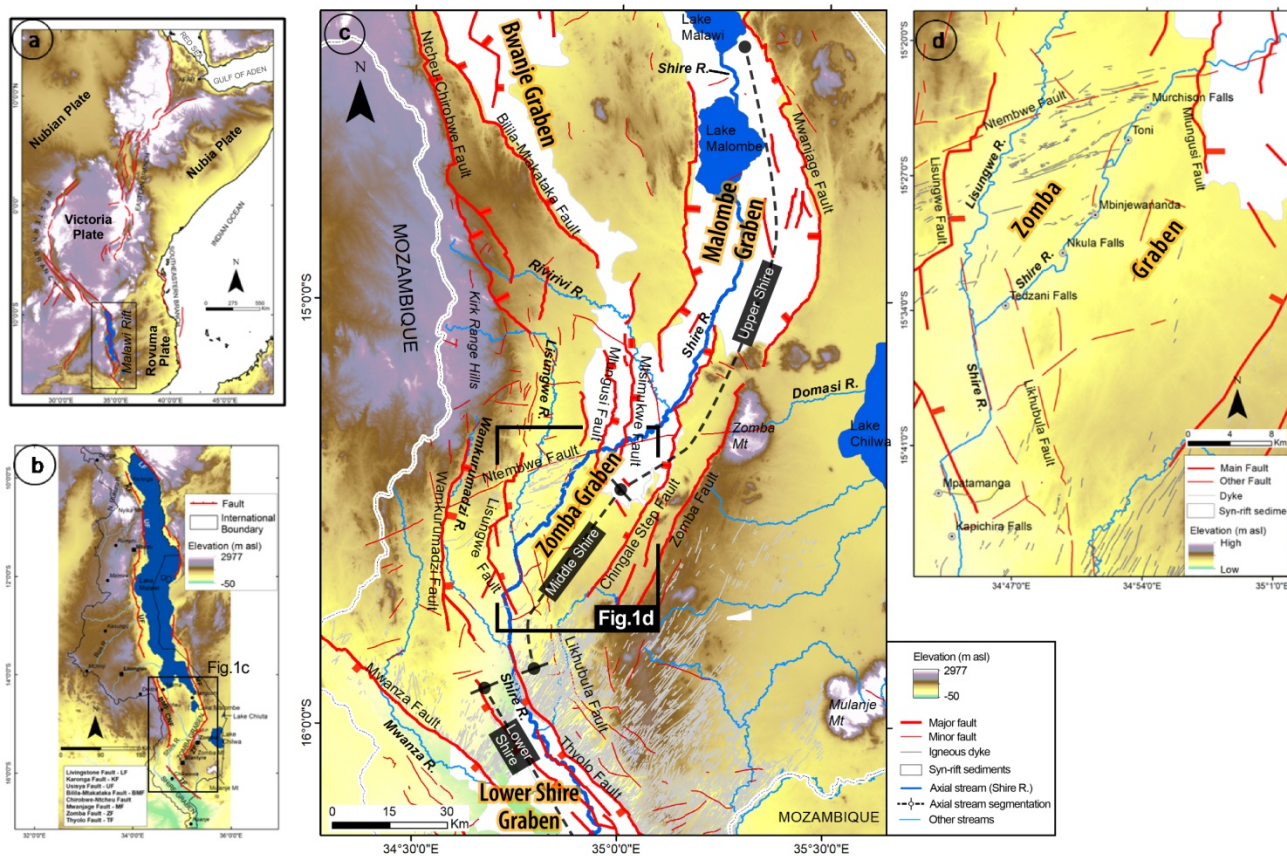
1109 Wobus, C., Whipple, K.X., Kirby, E., Snyder, N., Johnson, J., Spyropolou, K., Crosby,  
 1110 B., Sheehan, D., 2006. Tectonics from topography: procedures, promise, and pitfalls.  
 1111 *Geol. Soc. Am. Spec. Pap.* 398, 55–74.

1112 Woolley, A.R., 2001. Alkaline Rocks and Carbonatite of the World. Geological Society of  
 1113 London, pp. 158-177.

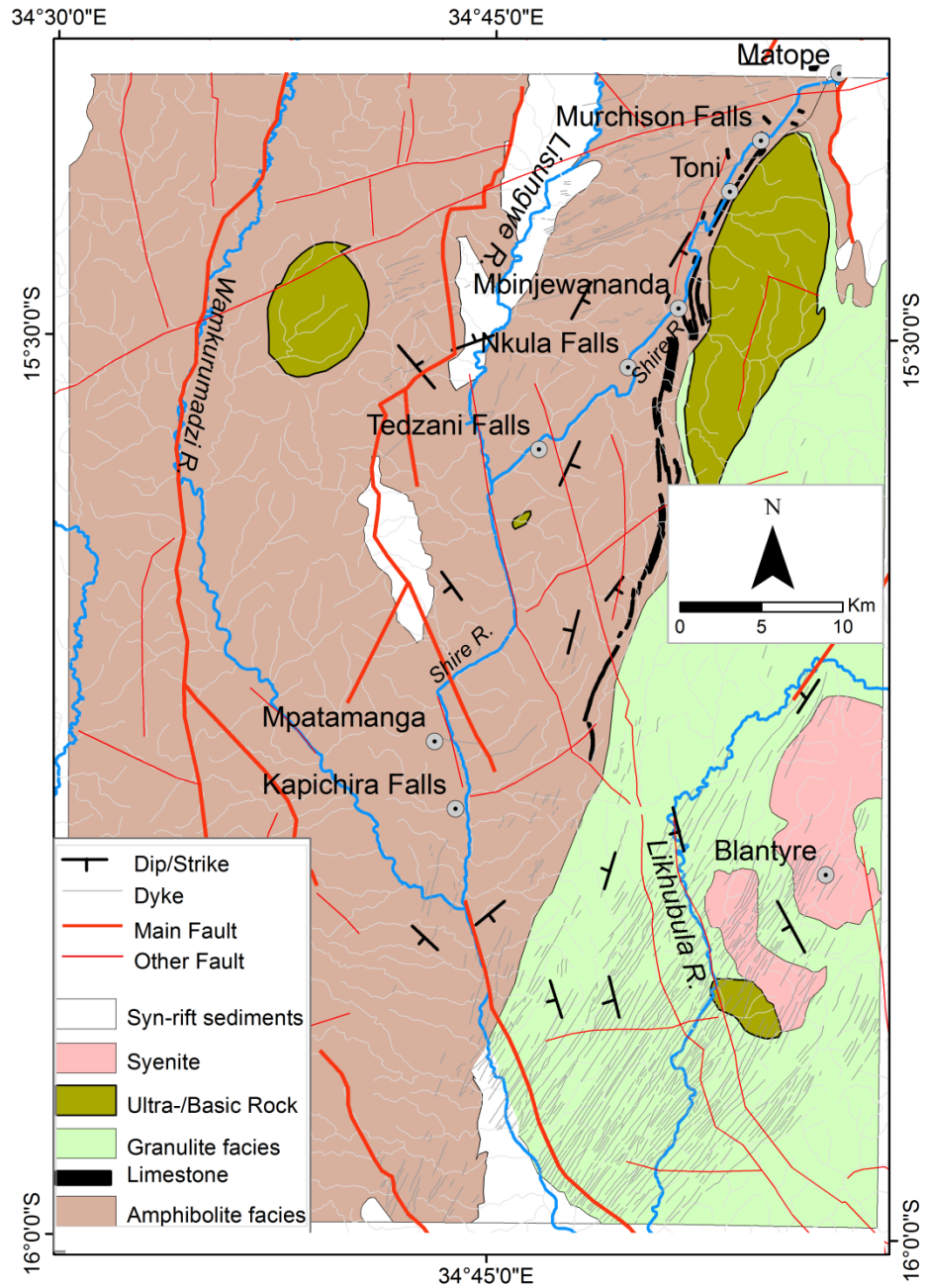
1114 Zahra, T., Paudel, U., Hayakawa, Y. S., and Oguchi, T., 2017. Knickzone Extraction  
1115 Tool (KET) - A new ArcGIS toolset for automatic extraction of knickzones from a DEM  
1116 based on multi-scale stream gradients, *Open Geosciences* 9, 73–88.

1117 Zhang, H., Kirby, E., Pitlick, J., Anderson, R. S., Zhang, P., 2017. Characterizing the  
1118 transient geomorphic response to base-level fall in the northeastern Tibetan Plateau.  
1119 *Journal of Geophysical Research: Earth Surface* 122, 546–572.

1120 **FIGURES**



1121  
 1122 Figure 1. The position of Malawi on the African continent (a) with the main tectonic features (adopted from Chorowicz,  
 1123 2005); The Malawi Rift (b) overlaid on an SRTM DEM showing the main geomorphological and tectonic  
 1124 features; The study area (c) showing the Shire River and the major tectonic elements (modified after Williams et al, 2022)  
 1125 and; (d) Some falls and rapids in the Middle Shire River section and the associated topographical and structural features.

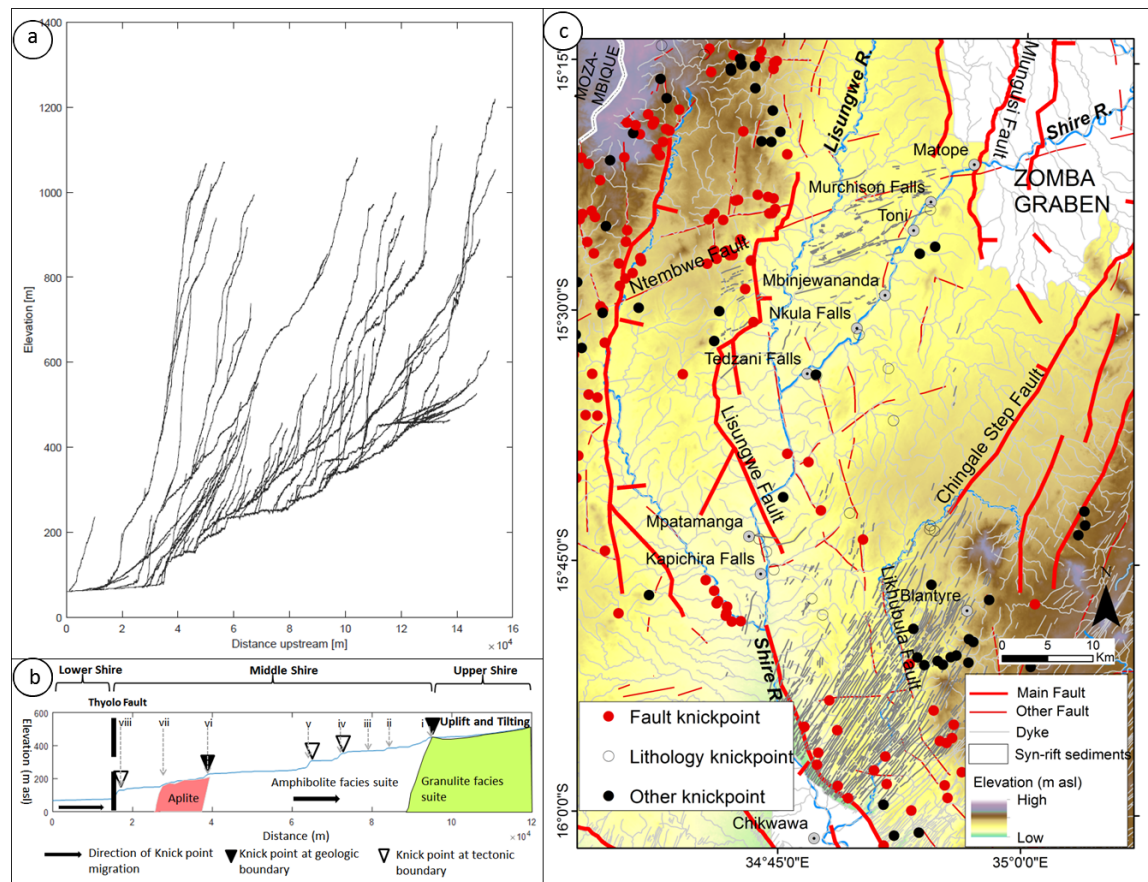


1126

1127 Figure 2. Detailed geology of the study area (modified after Habgood and Wa  
 1128 1965; Bloomfield and Garson, 1965; Evans, 1965; Habgood, 1963; Coope  
 1129 Bloomfield, 1961; Morel,



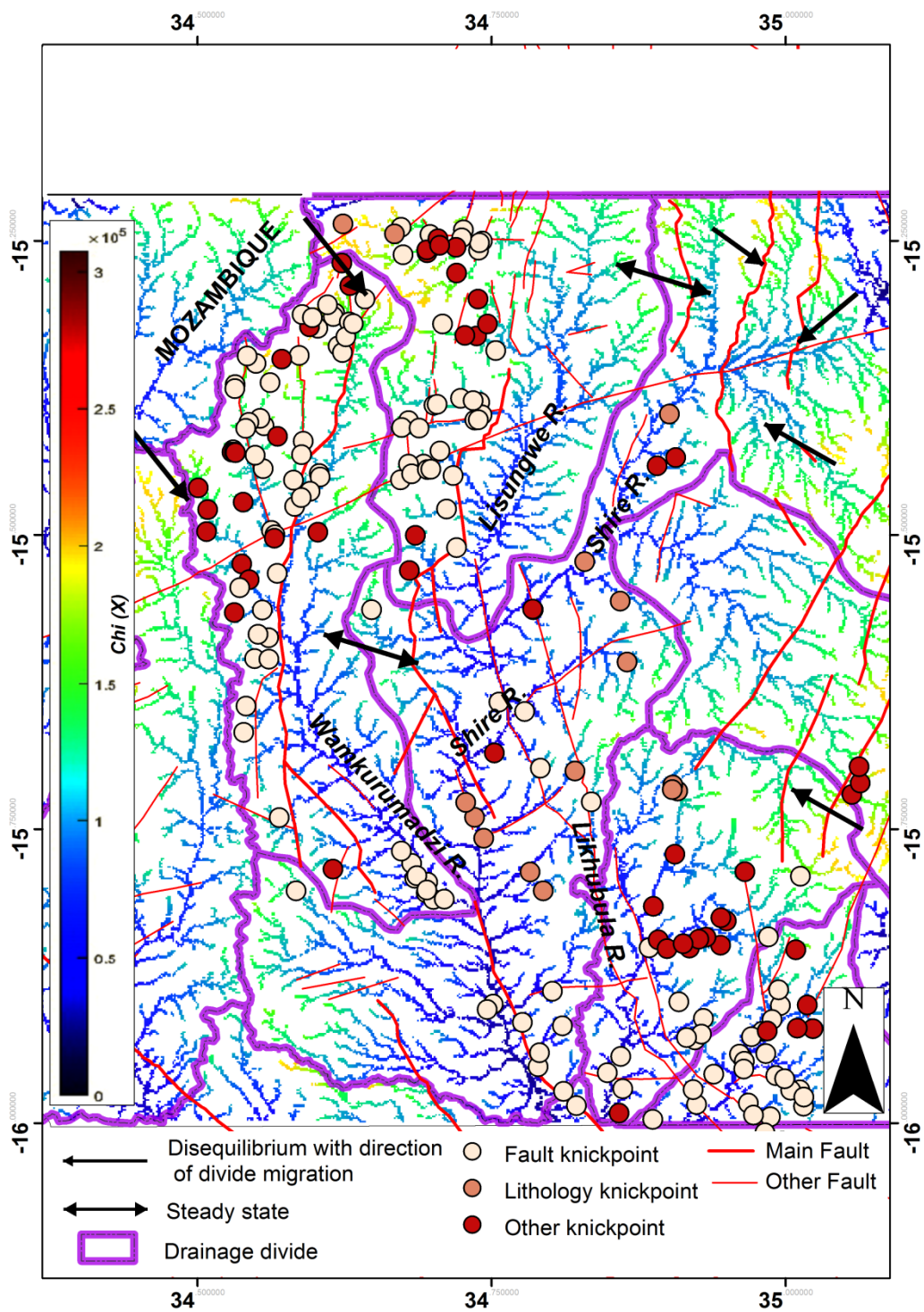
1130



1131

1132 Figure 3. Longitudinal profiles along: (a) the Middle Shire basin (b) the Middle Shire River with various knickpoints (i –  
 1133 Murchison Falls. ii – Toni-Nachimbeya Rapids. iii – Mbinjewananda Rapids. iv – Nkula Falls. v – Tedzani Falls. vi –  
 1134 Mpatamanga Gorge. vii – Mzimba Rapids. viii – Kapichira Falls) and some tectonic and lithological controls associated with

1136



1137

1138 Figure 4.  $\chi$ -plot of streams in (a) the Middle Shire Basin.

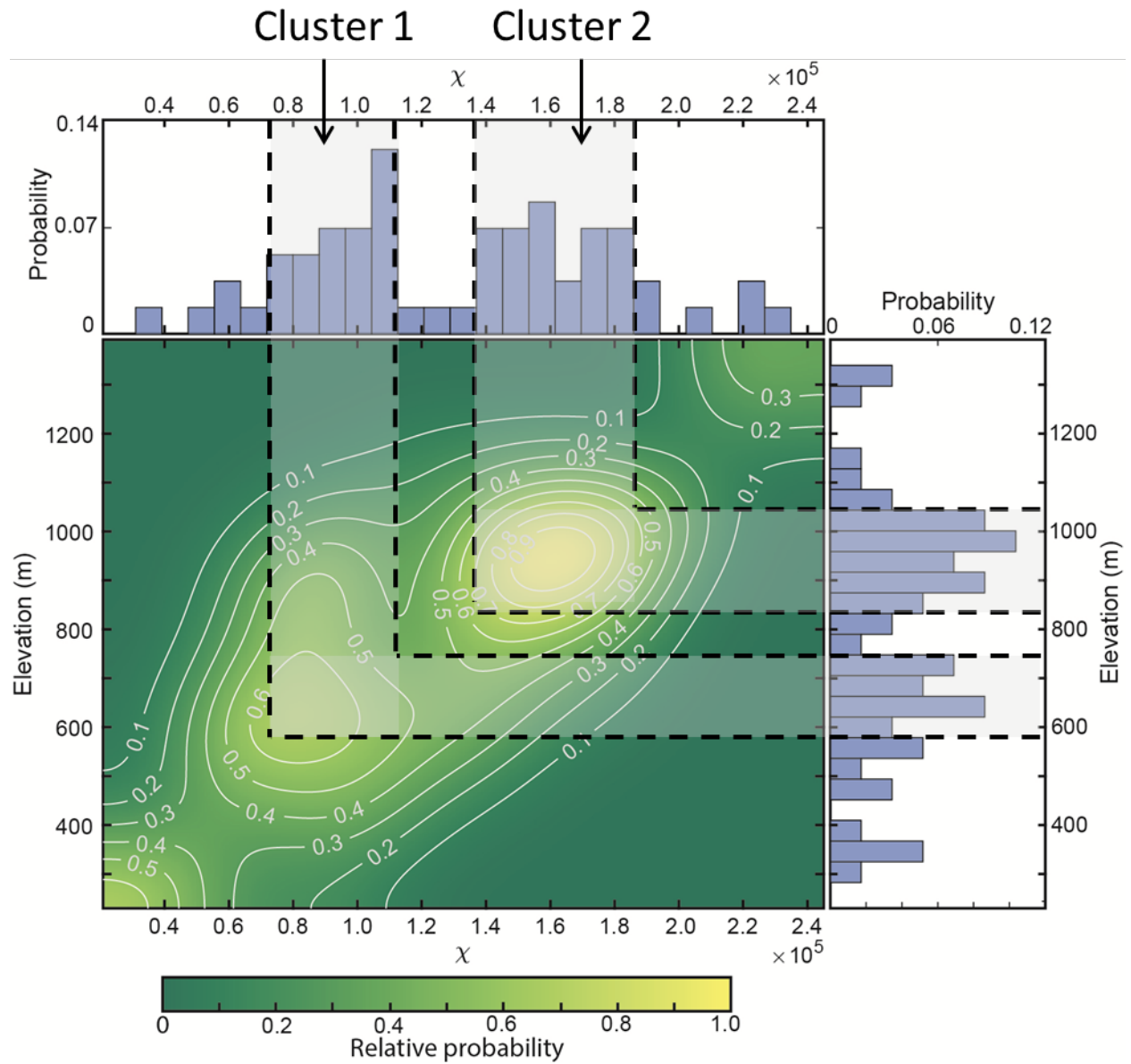
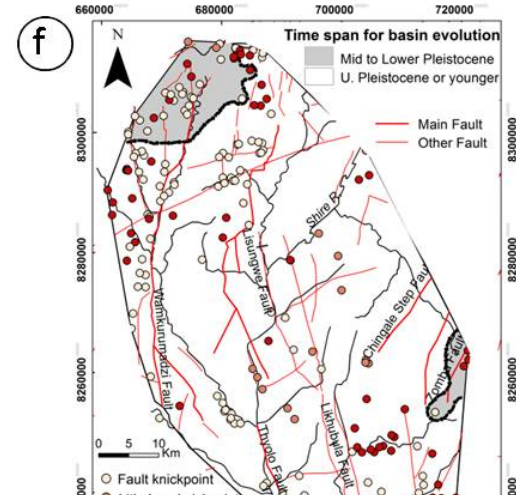
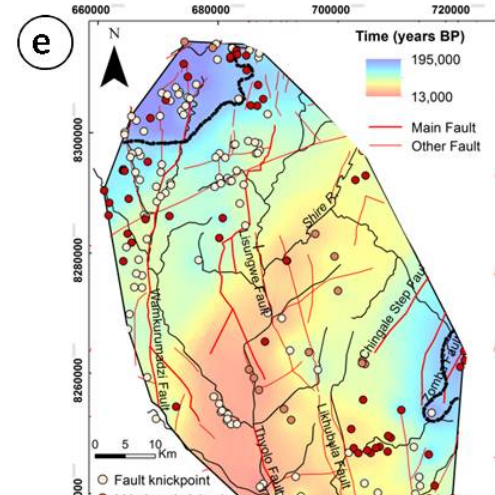
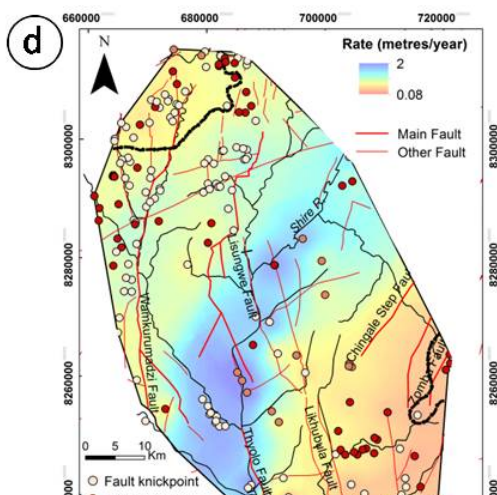
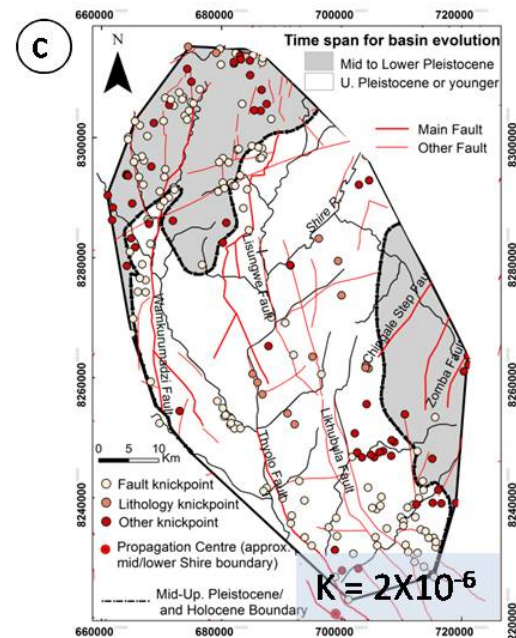
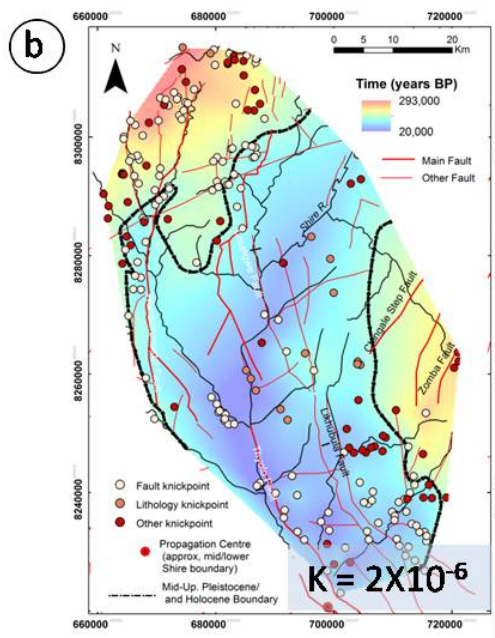
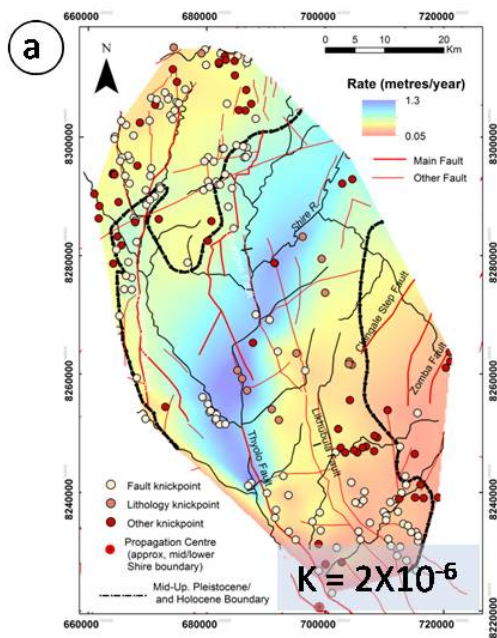


Figure 5. Chi-Elevation histogram probability plot and the associated knickpoint clusters.





1142 Figure 6. Knickpoint rates (a and d), response times (b and e) from different erodibility values (according to Jess et al.,  
1143 2021) and time spans for basin evolution (c and f) in the Middle Shire section. The legend for the knickpoints only  
1144 describes our observations of knickpoint associations, and that fault and lithology-related knickpoints are interpreted as  
1145 'static knickpoints' and 'others' are interpreted to be 'mobile knickpoints

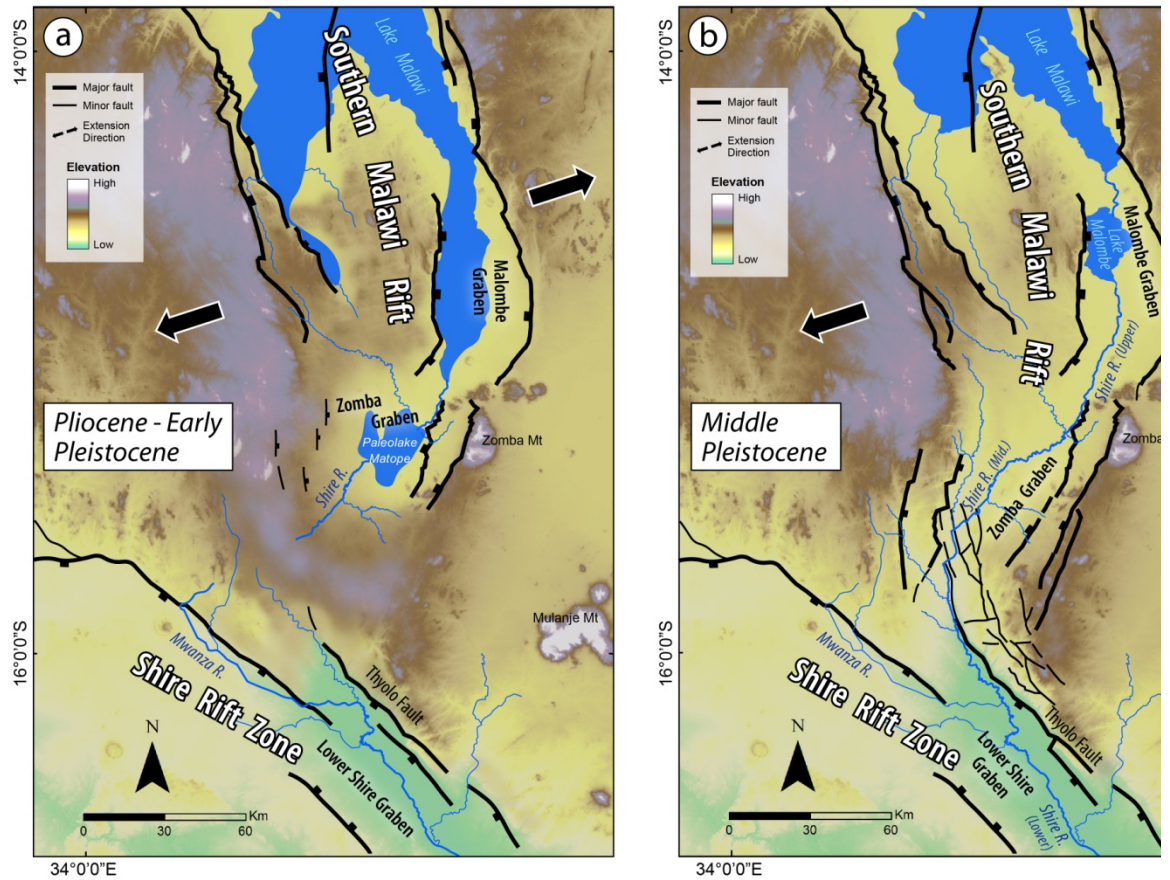


Figure 7. Hypothetical paleogeographical reconstruction of the Middle Shire rift into zone from (a) the Pliocene-Early Pleistocene to (b) the Middle Pleistocene and present day, connecting the Zomba Graben (in Southern Malawi Rift) and the Lower Graben (in Shire Rift Zone), after Dulanya (2017), Kolawole et al. (2021, 2022); and et al. (2022a,b).